

A comparative study on the apatite and zircon from the ore-related and -barren magmatic rocks of the Shatanjiao region, Lower Yangtze River Belt: Controlling effects for petrogenesis and Cu-Au mineralization

Yu Wang, Jing-ya Cao, Sheng-xiong Yang, Xiao-yong Yang, Majid Ghasemi Siani, Asghar Dolati, Muhammad Hafeez

Citation: Yu Wang, Jing-ya Cao, Sheng-xiong Yang, Xiao-yong Yang, Majid Ghasemi Siani, Asghar Dolati, Muhammad Hafeez, 2026. A comparative study on the apatite and zircon from the ore-related and -barren magmatic rocks of the Shatanjiao region, Lower Yangtze River Belt: Controlling effects for petrogenesis and Cu-Au mineralization, China Geology, 9, 120-135. doi: 10.31035/cg2024105.

View online: https://doi.org/10.31035/cg2024105

Related articles that may interest you

Geology and mineralization of the Tiegelongnan supergiant porphyry-epithermal Cu (Au, Ag) deposit (10 Mt) in western Xizang, China: A review

China Geology. 2022, 5(1), 136 https://doi.org/10.31035/cg2022001

Geology and mineralization of the Duobaoshan supergiant porphyry Cu-Au-Mo-Ag deposit (2.36 Mt) in Heilongjiang Province, China: A review

China Geology. 2023, 6(1), 100 https://doi.org/10.31035/cg2023006

Geology and mineralization of the Dongping supergiant alkalic-hosted Au-Te deposit (>100 t Au) in Northern Hebei Province, China: A review

China Geology. 2024, 7(3), 533 https://doi.org/10.31035/cg2023097

In situ U-Pb dating and trace elements of magmatic rutile from Mujicun Cu-Mo deposit, North China Craton: Insights into porphyry mineralization

China Geology. 2024, 7(4), 730 https://doi.org/10.31035/cg2023038

Geology and mineralization of the supergiant Shimensi granitic-type W-Cu-Mo deposit (1.168 Mt) in northern Jiangxi, South China: A Review

China Geology. 2022, 5(3), 510 https://doi.org/10.31035/cg2022036

Metallogenic characteristics of Shitoukengde intrusion and its implications for Ni-Co-(Cu) sulfide mineralization in East Kunlun

China Geology. 2024, 7(4), 714 https://doi.org/10.31035/cg2023070

China Geology 9 (2026) 120−135

China Geology

Journal homepage: http://chinageology.cgs.cn
https://www.sciencedirect.com/journal/china-geology



A comparative study on the apatite and zircon from the ore-related and -barren magmatic rocks of the Shatanjiao region, Lower Yangtze River Belt: Controlling effects for petrogenesis and Cu-Au mineralization

Yu Wang[a], Jing-ya Cao[b,*], Sheng-xiong Yang[b], Xiao-yong Yang[c], Majid Ghasemi Siani[d], Asghar Dolati[d], Muhammad Hafeez[c]

[a] *MNR Key Laboratory of Metallogeny and Mineral Assessment, Institute of Mineral Resources, Chinese Academy of Geological Sciences, Beijing* 100037, *China*
[b] *Southern Marine Science and Engineering Guangdong Laboratory (Guangzhou), Guangzhou* 511458, *China*
[c] *CAS Key Laboratory of Crust-Mantle Materials and Environments, University of Science and Technology of China, Hefei* 230026, *China*
[d] *Department of Geochemistry, Faculty of Earth Sciences, Kharazmi University, Tehran* 1571914911, *Iran*

ARTICLE INFO

Article history:
Received 14 June 2024
Received in revised form 3 March 2025
Accepted 19 March 2025
Available online 1 December 2025

Keywords:
Sr-Nd-Hf isotopes
Zircon U-Pb dating
Apatite Sr-Nd isotopes
Oxygen fugacity
Magma source
Adakitic rocks
Cu-Au mineralization
Shatanjiao Orefield

ABSTRACT

The links between the adakitic rocks and Cu-Au mineralization have long been argued. This study investigates petrogenesis and its link to mineralization potential by a series of *in-situ* geochronological and geochemical signatures of apatite and zircon in three ore-related intrusions and one-barren intrusion in the Middle-Lower Yangtze River Metallogenic Belt (MLYRB). Zircon U-Pb dating yield ages of 139–143 Ma and 121 Ma for the ore-related and ore-barren intrusions, respectively. The ore-related rocks have higher apatite Sr/Y (1.57–9.69), $(La/Yb)_N$ (16.7–159.5), and δEu (0.45–0.74) than the ore-barren rocks of 0.57–1.02, 19.3–24.1 and 0.40–0.45, respectively, indicating the former has an adakitic affinity, while the latter has a non-adakitic affinity. The ore-related rocks have enriched zircon Hf isotopes with $\varepsilon_{Hf}(t)$ values of −15.9 to −5.5 and T_{DMC} ages of 2408–1655 Ma and apatite Sr-Nd isotopes, indicating that the ore-related magmas were mainly originated from partial melting of subducted oceanic crust. The ore-barren rocks have higher $\varepsilon_{Hf}(t)$ values of −6.6 to −4.6 and lower T_{DMC} ages of 1598–1469 Ma and apatite Sr-Nd isotopes, indicating a lithospheric mantle source. The ore-related rocks have higher oxygen fugacity of mean ΔFMQ+2.00 and X_F/X_{OH} of 8.36–175 than the ore-barren rocks of mean ΔFMQ+1.43 and 3.72–4.96. It was inferred that magma source, water content, and oxygen fugacity emerge as critical factors governing the regional Cu-Au mineralization potential.

©2026 China Geology Editorial Office.

1. Introduction

Adakitic rocks share similar geochemical signatures with these adakites and are characterized by SiO_2 contents ⩾ 56%, Al_2O_3 contents ⩾ 15%, elevated Sr abundances (> 400 $\times10^{-6}$), and depleted Y (< 18 $\times10^{-6}$) and Yb (< 1.9 $\times10^{-6}$) contents (Defant MJ and Drummond MS, 1990; Defant MJ and Kepezhinskas P, 2001). Adakites, characterized by their distinctive geochemistry, are widely attributed to the partial melting of subducted oceanic crust (Richards JR and Kerrich R, 2007; Richards JP, 2011). In contrast, adakitic rocks, which share geochemical similarities with adakites, can form through diverse mechanisms, including the partial melting of thickened or delaminated lower continental crust, as observed in settings such as the Dabie Mountains, the Qinghai-Xizang Plateau, and the North China Craton (Chung SL et al., 2003; Gao S et al., 2004; Wang Q et al., 2007a; Liu SA et al., 2010). Additionally, fractional crystallization of garnet, hornblende, titanite, and zircon from typical arc magmas, as well as mixing between crustal and mantle-derived melts, can also yield adakitic compositions (Castillo PR et al., 1999; Richards JP and Kerrich R, 2007; Li JW et al., 2009; Richards JP, 2011). Despite the multifaceted nature of their petrogenesis, a compelling link exists between adakitic magmatism and porphyry-skarn mineralization which is widely recognized within the scientific community (Sajona FG and Maury RC,

First author: *E-mail address*: geowangyu@mail.ustc.edu.cn (Yu Wang).
* Corresponding author: *E-mail address*: jingyacao@126.com (Jing-ya Cao).

Literary editor: Li-qiong Jia
doi:10.31035/cg2024105
2096-5192/© 2026 China Geology Editorial Office.

1998; Sun WD et al., 2010; Richards JP, 2011; Sun et al., 2015; Deng JH et al., 2016, 2017; Xie F et al., 2018; Wang Y et al., 2022a). The Tongling ore-cluster region, a representative segment of the Middle-Lower Yangtze River Metallogenic Belt (MLYRB), hosts a series of Yanshanian intrusive complexes. These complexes include adakitic intrusions spatially and temporally associated with porphyry-skarn deposits, as well as ore-barren non-adakitic intrusions (Wang Y et al., 2022b). Despite this association, the petrogenesis of these rocks and the critical factors governing mineralization remain subjects of ongoing debate.

Apatite [$Ca_5(PO_4)_3(F, OH, Cl)$], a ubiquitous accessory mineral in igneous rocks, serves as a repository for a diverse array of elements, including volatiles (F and Cl), multivalent elements (e.g., Fe, Mn, Ga, Ce, Eu, and S), and trace elements (e.g., Sr, Mg, and REEs) (Sha LK and Chappell BW, 1999; Pan YM and Fleet ME, 2002). The stability of apatite during subsequent geological processes makes it an ideal geochemical tracer, whose robust nature allows researchers to estimate the oxygen fugacity and volatile content of the parental magma, identify the rock's petrogenetic affinity, and trace the magmatic source and evolutionary trajectory (Miles AJ et al., 2014; Pan LC et al., 2016; Bruand E et al., 2017; Laurent O et al., 2017; Cao JY et al., 2022, 2023; Ma Y et al., 2023). Zircon is another common accessory mineral in magmatic rocks and usually unaffected by hydrothermal alteration in mineralization system. Previous studies have proposed various methods to calculated oxygen fugacity (f_{O_2}) by using trace elements Ce and Eu in zircon (Ballard JR et al., 2002; Trail D et al., 2012). Although the oxidation state when zircon crystillized are also affected by temperature, pressure, and parental melt composition, Loucks RR et al. (2020) presented a new method to estimate the magmatic oxybarometer, which can directly calculate the absolute value of f_{O_2} from values of ΔFMQ based on zircon trace element analysis.

The Shatanjiao Orefield, situated within the MLYRB, hosts a suite of porphyry-skarn Cu-Au mineralized and barren intrusions. Despite their significance, comparative studies about the petrogenesis and magmatic physical-chemical conditions between the two intrusion types are scarce. This study investigates the petrogenesis and magmatic evolution of four intrusions within the Shatanjiao Orefield of the Tongling ore cluster: three ore-related intrusions (Jinziwei, Yaojialing, and Guihuachong) and an ore-barren granite porphyry. The authors present a comprehensive geochemical dataset, including major and trace element compositions, Sr-Nd isotopic ratios of apatite, zircon U-Pb ages, trace element and Lu-Hf isotopic compositions. This multi-faceted approach aims to: (1) Evaluate the efficacy of apatite as a tracer for the identification of adakitic rocks and magma sources; (2) constrain the magmatic oxygen fugacity during emplacement; and (3) elucidate the implications for porphyry-skarn Cu-Au mineralization.

2. Geological setting

The Middle-Lower Yangtze River Metallogenic Belt

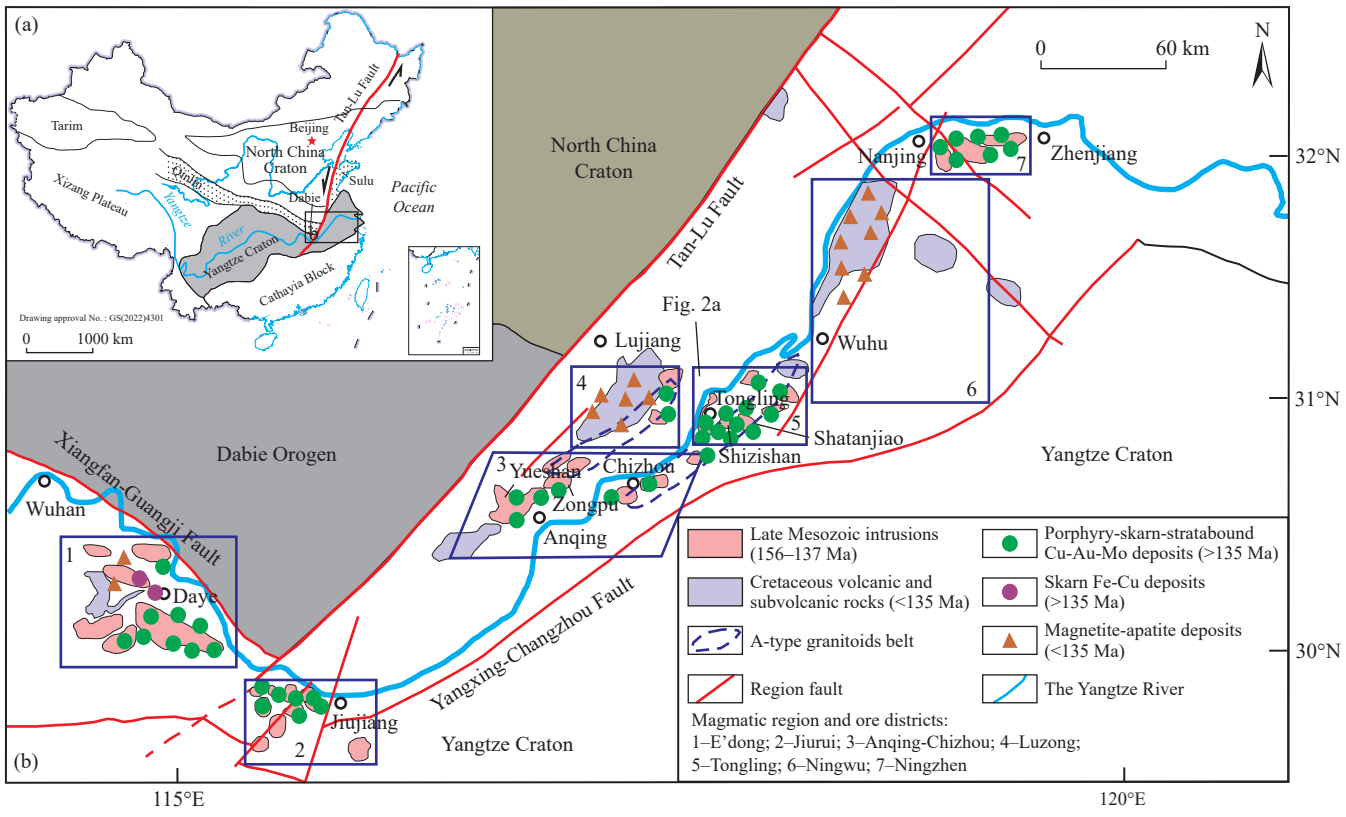


Fig. 1. Regional geological sketch map showing the distribution of major mining districts along the Yangtze River in East China and the location of the Shatanjiao Orefield (modified from Pan Y and Dong P, 1999).

(MLYRB), located in eastern China along the northern margin of the Yangtze Craton, is renowned for its Cu-Fe-Au polymetallic mineralization (Fig. 1a). Bounded by the Xiangfan-Guangji Fault to the southwest, the Tancheng-Lujiang Fault to the northwest, and the Yangxin-Changzhou Fault to the southeast, the MLYRB hosts seven prominent ore clusters: E'dong, Jiurui, Anqing-Guichi, Luzong, Tongling, Ningwu, and Ningzhen (Fig. 1b). Cu polymetallic mineralization within the MLYRB is predominantly associated with Late Jurassic–Early Cretaceous intermediate-felsic magmatism. These intrusions are emplaced within a complex basement assemblage comprising Neoproterozoic low-grade metamorphic rocks and Paleozoic to Triassic sedimentary sequences (Jiang XY et al., 2020; Yan J et al., 2021). The sedimentary succession, consisting primarily of clastic rocks, carbonates, mudstones, and argillaceous limestones, provides favorable lithological and structural controls for porphyry-skarn-type Cu-Fe-Au mineralization (Chang YF et al., 1991; Xie JC et al., 2008). The oldest exposed basement rocks within the MLYRB are the Proterozoic–Archean (⩾ 3.5 Ga) Douling Complex, which is composed of amphibolite-facies gneisses, schists, and amphibolites (Zhang SB et al., 2006; Zhang SB and Zheng YF, 2013).

The Shatanjiao Orefield, located within the eastern Tongling ore cluster region (Fig. 1b), hosts a series of porphyry-skarn-type Zn-Cu-Au polymetallic deposits. These deposits are spatially and temporally associated with three distinct granodiorite intrusions (including porphyritic facies): The Shatanjiao, Yaojialing, and Guihuachong intrusions, which are distributed from west to east, respectively (Fig. 2). A granite porphyry dike is also observed between the Shatanjiao and Yaojialing intrusions. Exposed sedimentary strata within the Shatanjiao Orefield encompass a range of Paleozoic, Mesozoic, and Quaternary units. These include Silurian and Devonian quartz sandstones, Carboniferous carbonates, Permian shales, Triassic carbonates, Jurassic-Cretaceous sandstones and siltstones, and Quaternary glutenites (Fig. 2). The region has been significantly affected by Mesozoic tectonic events, specifically the Indosinian and Yanshanian orogenies, resulting in the formation of numerous folds and faults (Huang WM et al., 2019). Fault systems within the orefield exhibit predominantly NE- and NW-trending orientations (Fig. 2). Several skarn Cu-Au deposits

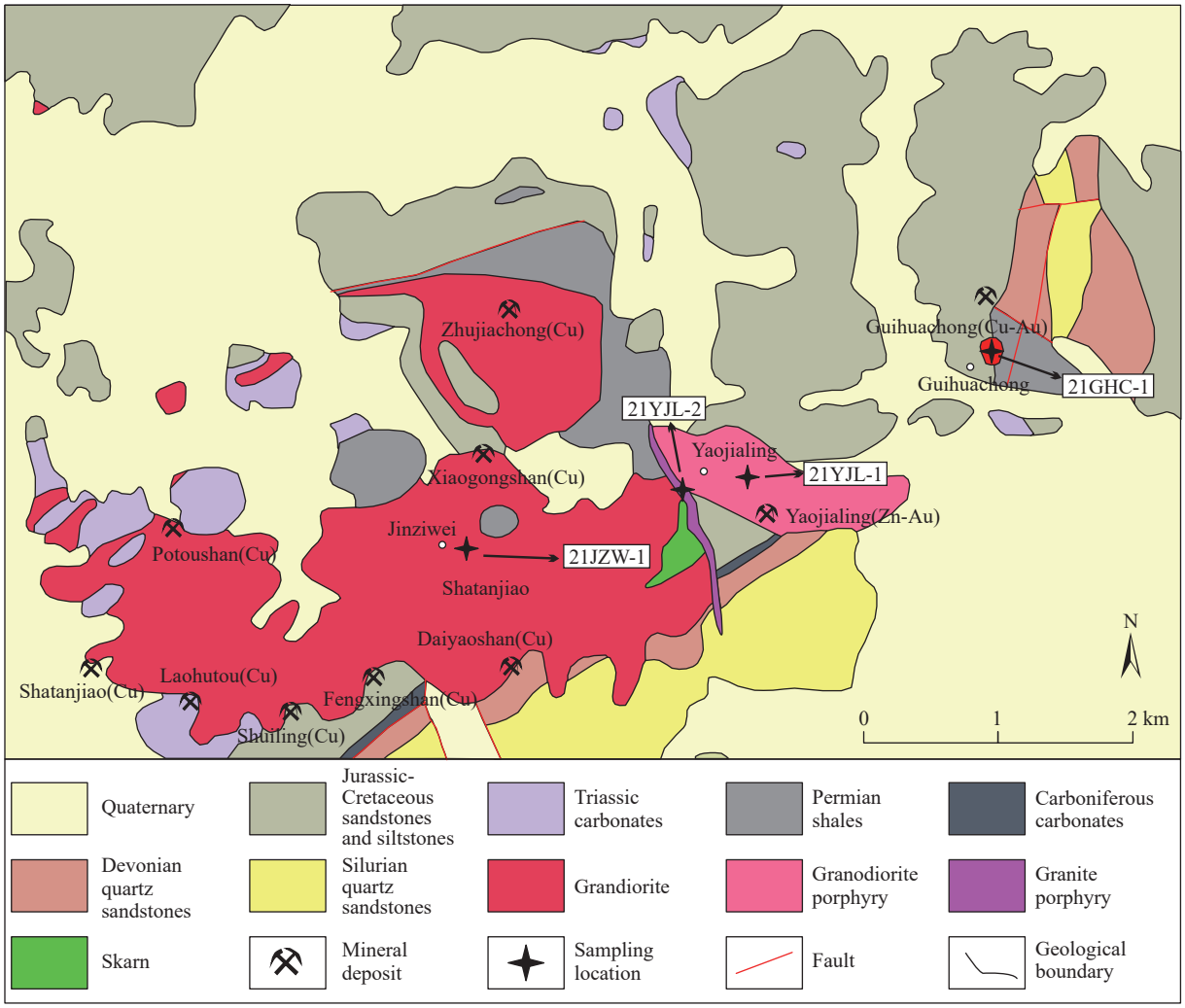


Fig. 2. Geological sketch map of the Shatanjiao Orefield, showing the locations of the Shatanjiao, Yaojialing and Guihuachong intrusions (modified from Huang WM et al., 2019).

are hosted within the Shatanjiao intrusion, primarily occurring at the contact zone between the intrusion and surrounding carbonate formations. These deposits, characterized by surface exposure of skarn mineralization, include Xiaogongshan, Daiyaoshan, Shatanjiao, Zhujiachong, Shuiling, Potoushan, and Fengxingshan (Fig. 2). West of the Shatanjiao intrusion, separated by the aforementioned granite porphyry dike, lies the Yaojialing granodiorite porphyry intrusion. This intrusion hosts the significant Yaojialing Zn-Cu-Au deposit, a large-scale porphyry-skarn system. Further east, the Guihuachong granodiorite intrusion hosts a typical porphyry-type Cu-Au deposit (Fig. 2).

3. Sample descriptions and analytical methods

3.1. Sample description

Four samples were collected from the Shatanjiao Orefield, including two granodiorite samples from the Guihuachong and Jinziwei intrusions, a granodiorite porphyry and a granite porphyry samples from the Yaojialing intrusion. The granodioritic rocks are ore-related rocks and the granite porphyry is ore-barren rocks. The detailed sampling location is shown in Fig. 2.

The granodiorite sample (21GHC-1) from the Guihuachong intrusion is light gray, subhedral to euhedral with medium- to fine-grained texture and massive structure (Figs. 3a, b). They are mainly composed of plagioclase (40–45 vol%), quartz (about 20 vol%), hornblende (5–10 vol%), biotite (about 10 vol%), and accessory minerals such as zircon, apatite, and titanite. While the granodiorite sample (21JZW-1) from Jinziwei shows a medium- to coarse-grained structure, other characteristics are similar to those from Guihuachong (Figs. 3c–d). The granodiorite-porphyry sample (21YJL-1) from the Yaojialing intrusion is light gray and displays a massive structure and porphyritic texture (Fig. 3e). It is composed of phenocrysts and matrix (Fig. 3f). Phenocrysts mainly consist of plagioclase (about 45 vol%), K-feldspar (about 25 vol%), quartz (about 20 vol%), hornblende (about 5 vol%) and biotite (about 5 vol%) (Fig. 3f). The mineral assemblages of the matrix are similar to the phenocrysts, but the size is much lower than the phenocrysts. The accessory minerals are mainly zircon, apatite, and magnetite.

The granite porphyry (21YJL-2) from Yaojialing is also porphyritic and contains phenocrysts of plagioclase (40–45 vol%), quartz (about 30 vol%), K-feldspar (about 20 vol%) and biotite (about 5 vol%) (Fig. 3g). The accessory minerals are mainly zircon and apatite, which mainly occur as inclusions in biotite (Fig. 3h).

3.2. Zircon U-Pb dating, trace element and Lu-Hf isotope analyses

Zircon U-Pb dating and trace element compositions were performed using laser ablation-inductively coupled plasma-mass spectrometry (LA-ICP-MS) at the *in situ* Mineral Geochemistry Lab, Ore Deposit and Exploration Centre (ODEC) of Hefei University of Technology, China. Analyses were conducted using an Agilent 7900 quadrupole ICP-MS coupled with a Photon Machines Analyte HE 193 nm ArF excimer laser ablation system. Ablation was performed in a high-purity helium (UHP He) atmosphere at a flow rate of 0.90 L/min. The ablated aerosol was mixed with argon (Ar) at a flow rate of 0.85 L/min immediately after exiting the ablation cell. The ICP-MS system was optimized daily for sensitivity in the desired mass range while minimizing the production of molecular oxide species (typically < 0.3%) (Wang FY et al., 2017).

Following U-Pb dating and trace element content, *in-situ* Lu-Hf isotopic analyses were conducted on the same zircon domains using a New Wave 193 nm ArF-excimer laser ablation system coupled to a Neptune multi-collector inductively coupled plasma mass spectrometer (LA-MC-ICP-MS) at the Tianjin Institute of Geology and Mineral Resource, Chinese Academy of Geological Sciences. Detailed methodologies can be referenced in Deng JH et al. (2017).

3.3. EPMA and in-situ LA-ICP-MS trace element analysis of apatite

Major element compositions of apatite were determined using a JEOL JXA–8230 electron microprobe at the School of Resources and Environmental Engineering, Hefei University of Technology, China. Analyses were conducted with an accelerating voltage of 15 kV, a beam current of 8 nA, and a beam diameter of 5 μm. The following elements were measured: F, Na, Mg, Al, P, Cl, K, Ca, Ti, Mn, Fe, and Ce.

Trace element concentrations in apatite were measured via laser ablation inductively coupled plasma-mass spectrometry (LA-ICP-MS). Analyses were performed at the School of Resources and Environmental Engineering, Hefei University of Technology, China, utilizing a Resonetics 193 nm ArF-Excimer laser coupled with an Agilent 7500a ICP-MS instrument. A laser beam diameter of 30 μm and a frequency of 5 Hz were employed, with an energy level of 4 J/cm^2. Each analysis consisted of a 20-second gas blank measurement followed by a 40-second sample ablation period. Standard reference materials SRM 610 and BCR–2G were used for calibration and quality control. Offline data processing was conducted using ICPMSDataCal (Liu YS et al., 2008). The mole fractions of F, Cl, and OH in apatite (X_F, X_{Cl}, and X_{OH}) were calculated based on the model proposed by Li WR and Costa F (2020).

3.4. In-situ LA-MC-ICP-MS strontium and neodymium isotopic analysis of apatite

Strontium (Sr) and neodymium (Nd) isotopic compositions of apatite were measured using a Thermo Fisher Scientific Neptune Plus multi-collector inductively coupled plasma mass spectrometer (MC-ICP-MS) coupled with a Coherent GeoLas HD excimer ArF laser ablation system at

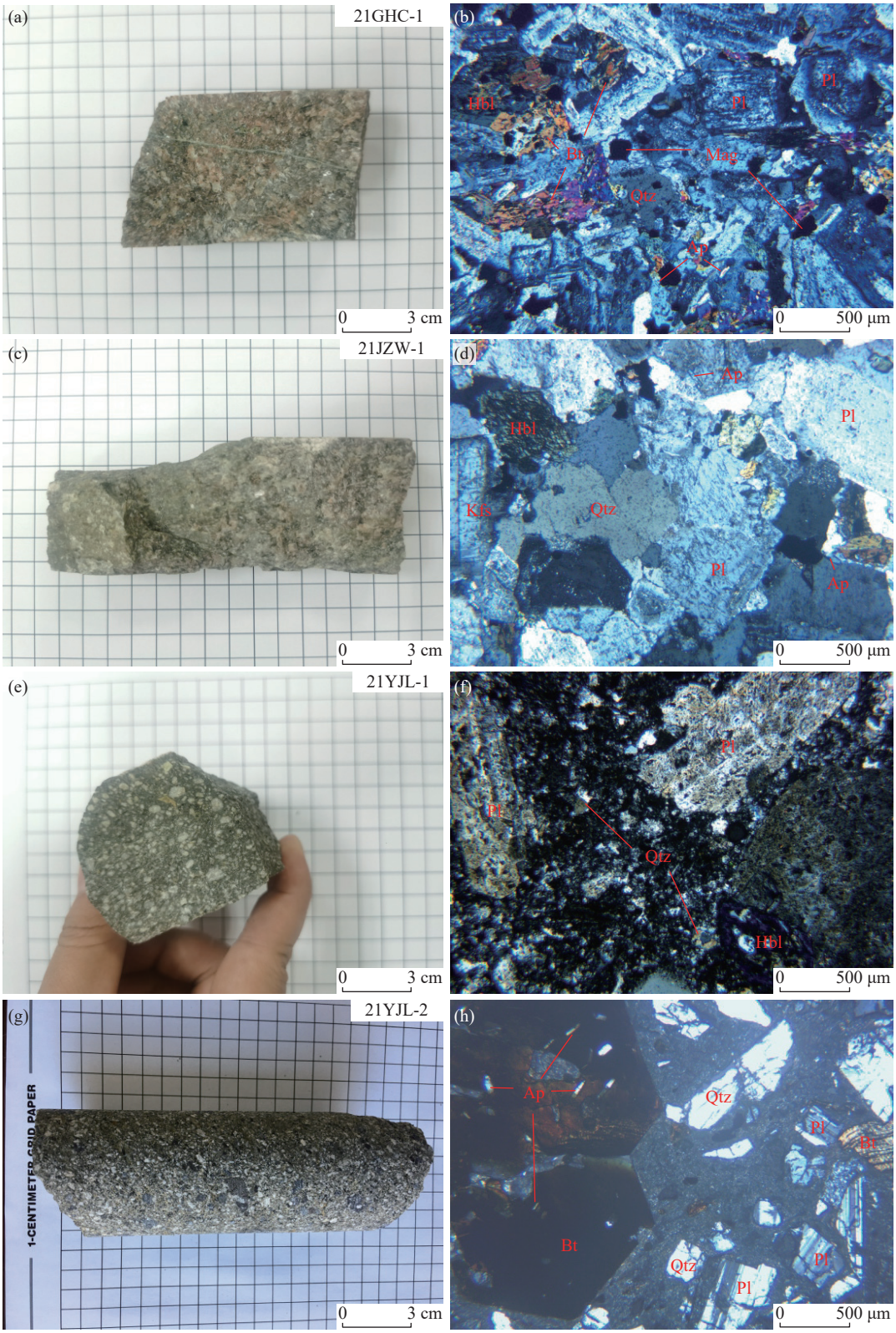


Fig. 3. Hand specimens (a, c, e, g) and photomicrographs (b, d, f, h) of the Shatanjiao Orefield. Bt–biotite; Hbl–hornblende; Kfs–K-feldspar; Pl–plagioclase; Qtz–quartz; Mag-magnetite; Ap-apatite.

Wuhan Sample Solution Analytical Technology Co. Ltd. (Wuhan, China). The Neptune Plus MC-ICP-MS was configured with nine Faraday cups (10^{11} Ω resistors) arranged to monitor Kr, Rb, Er, Yb, and Sr isotopes (L4 to H3). A high-sensitivity X-skimmer cone and Jet-sample cone were used. Helium was used as the carrier gas in the laser ablation system. Single-spot laser ablation was performed with a spot diameter of 60 μm, a pulse frequency of 8–15 Hz, and a laser fluence is about 10 J/cm^2.Data reduction for the LA-MC-ICP-MS analysis was performed utilizing ICPMSDataCal (Liu YS

et al., 2010). The Sr-Nd isotopic analysis methodology of apatite is detailedly described by Cao JY et al. (2023).

4. Results

4.1. Zircon U–Pb ages and trace elements

LA-ICP-MS zircon U–Pb age and trace elements data of the four samples in the Shatanjiao Orefield are listed in Supplementary Table S1. These euhedral zircon grains have lengths of 100–200 μm and aspect ratios of 2∶1 to 3∶1. In addition, these zircon grains are generally colorless, prismatic, and transparent and show microscale oscillatory zoning, suggesting a magmatic origin (Fig. 4; Hoskin PWO and Schaltegger U, 2003). Analyses of more than 20 spots yielded concordant U–Pb ages with weighted mean $^{206}Pb/^{238}U$ ages of 139.3 ± 0.6 Ma (MSWD = 1.3), 142.5 ± 1.5 Ma (MSWD = 1.6), and 140.8 ± 1.1 Ma (MSWD = 1.03) for samples 21GHC-1, 21JZW-1, and 21YJL-1, respectively (Figs. 4a–c), indicating Early Cretaceous formation ages, which are consistent with Yanshanian magmatic activity. The granite porphyry sample (21YJL-2) from Yaojialing was formed at 121.0 ± 2.8 Ma (MSWD = 1.3, n = 19), nearly 20 Ma years later than the granodiorite (porphyry) in the Shatanjiao Orefield (Fig. 4d).

Trace element contents of zircons (Table S1) in the Shatanjiao Orefield display that the Ti content of the zircons from the ore-related rocks and ore-barren rock range from 0.57×10^{-6} to 9.56×10^{-6} (average 3.24×10^{-6}) and 18.77×10^{-6} to 20.97×10^{-6} (19.79×10^{-6}), corresponding to temperature of 631°C to 876°C (average 760°C) and 956°C to 970°C (average 962°C) respectively (Ferry JM and Watson EB, 2007). The calculated oxygen fugacity parameter are from ΔFMQ+0.59 to ΔFMQ+3.41 and Eu/Eu* values from 0.50 to 0.88 for ore-related rocks, which is distinct different from that of ore-barren rock (ΔFMQ+1.22 to ΔFMQ+1.75; Eu/Eu*: 0.24 to 0.55).

4.2. Zircon Lu-Hf isotopes

LA-MC-ICP-MS zircon Lu-Hf isotope analyses for the four samples were carried out on zircon grains that had been analyzed for U-Pb ages, and the results are presented in Supplementary Table S2. Zircons from the Guihuachong granodiorite (21GHC-1) have $^{176}Hf/^{177}Hf$ ratios of 0.282169–0.282435. Based on the zircon age of 139 Ma for this sample, the calculated initial $^{176}Hf/^{177}Hf$ ratios range from 0.282148 to 0.282433, yielding corresponding $\varepsilon_{Hf}(t)$ values of

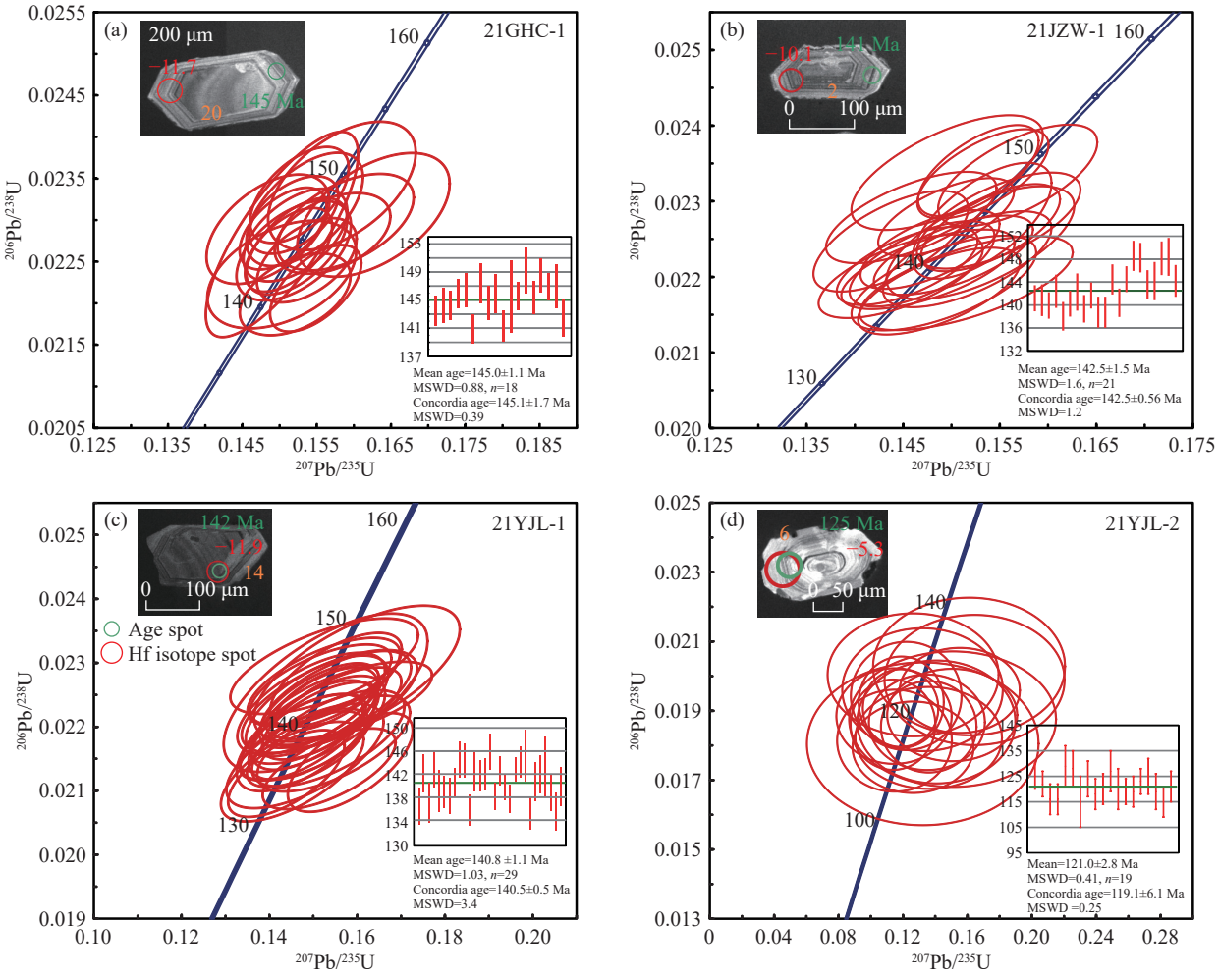


Fig. 4. CL images of representative zircon grains from Guihuachong (a), Jinziwei (b) and Yaojialing (c, d) intrusions in the Shatanjiao Orefield. The green circles and red circles represent analysis locations of zircon U-Pb ages and Hf isotope, respectively.

−12.9 to −7.8 and T_{DMC} ages of 2070–1758 Ma. Zircons from the Jinziwei granodiorite (21JZW-1) have $^{176}Hf/^{177}Hf$ ratios of 0.282274–0.282444. Based on the zircon age of 142 Ma for this sample, the calculated initial $^{176}Hf/^{177}Hf$ ratios range from 0.282272 to 0.282443, yielding corresponding $\varepsilon_{Hf}(t)$ values of −14.6 to −8.6 and T_{DMC} ages of 2119–1736 Ma. Based on the zircon age (141 Ma) of the granodiorite porphyry sample (21YJL-1) from Yaojialing, they have $^{176}Hf/^{177}Hf$ ratios of 0.282330–0.282437, yielding initial $^{176}Hf/^{177}Hf$ ratios of 0.282289 to 0.282479, corresponding $\varepsilon_{Hf}(t)$ values of −14.0 to −7.3 and T_{DMC} ages of 2078–1655 Ma. The zircon Hf isotopic compositions of the three samples are consistent within the error range, indicating a similar magmatic source. While zircons from the Yaojialing granite porphyry (21YJL-2) show significantly different Hf isotopic compositions, the calculated initial $^{176}Hf/^{177}Hf$ ratios range from 0.282510 to 0.282568, yielding corresponding $\varepsilon_{Hf}(t)$ values of −6.6 to −4.6 and T_{DMC} ages of 1527–1598 Ma (Fig. 5). In addition, the authors have found three captured zircons in two granodiorite samples from the Guihuachong and Jinziwei intrusions. The ages of these zircons are 646 Ma, 988 Ma, and 2007 Ma with $\varepsilon_{Hf}(t)$ values of −7.8, −2.7, and −6.1, respectively, indicating the assimilation of ancient crustal materials.

4.3. Apatite major and trace elements

The apatite grains are prismatic with smooth surfaces and have no oscillatory-zoned structure (Fig. 6). Those selected from the granodiorite (porphyry) samples are subhedral, have lengths of 50–200 μm and aspect ratios of 1.5∶1 to 2∶1, while those from the granite porphyry are euhedral and have relatively long lengths (100–200 μm) and aspect ratios of 2∶1 to 4∶1. The major and trace element compositions of apatite from the Shatanjiao Orefield are listed in Supplementary Table S3. Apatite in the four samples have CaO contents of 57.28%–61.50%, P_2O_5 contents of 36.09%–38.55%, variable F contents of 1.75%–3.90% and Cl contents of 0.02%–0.92% (Fig. 7). Most of the K_2O, TiO_2, and Al_2O_3 contents are below the detection limit.

Apatite samples in the granodiorite (porphyry) contain relatively higher Sr contents of (413–1250)×10^{-6} than that in granite porphyry of (701–963)×10^{-6}, whereas the former contains lower Y contents (77.8–374)×10^{-6} than the latter of (856–1486)×10^{-6}. The total rare earth element (ΣREE) contents of apatite in the granodiorite (porphyry) samples range from 2824×10^{-6} to 12432×10^{-6}, which are lower than granite porphyry samples of 18389×10^{-6} to 29033×10^{-6}. All samples are enriched in LREE relative to HREE (Fig. 8), however, the granodiorite (porphyry) samples have higher $(La/Yb)_N$ ratios of 16.7–159.5 and δEu values of 0.45–0.74 than the granite porphyry samples of 19.3–24.1 and 0.40–0.45, respectively.

4.4. Apatite Sr-Nd isotopes

In-situ Sr and Nd isotopic compositions of apatite in the four samples are given in Supplementary Table S4. Generally, the $^{87}Rb/^{86}Sr$ ratio of apatite is very low. Thus, the analyzed $^{87}Sr/^{86}Sr$ ratios can represent the initial $^{87}Sr/^{86}Sr$ ratios, and $\varepsilon_{Nd}(t)$ values of apatite are calculated based on the zircon U–Pb ages (140 Ma for 21GHC-1, 21JZW-1, and 21YJL-1; 120 Ma for 21YJL-2). The $^{87}Sr/^{86}Sr$ ratios and $\varepsilon_{Nd}(t)$ values of apatite from the three granodiorites (porphyries) range from 0.707501 to 0.708457 and −14.3 to −7.6, respectively, while those of granite porphyry range from 0.705718 to 0.706657 and −8.2 to −6.7, respectively (Fig. 9).

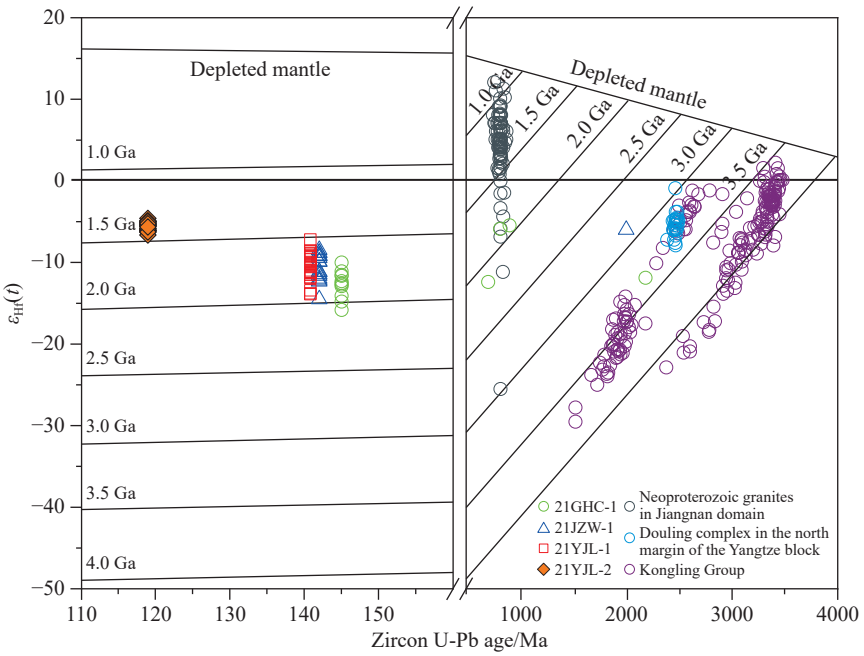


Fig. 5. $\varepsilon_{Hf}(t)$ *vs.* zircon U-Pb age of the Shatanjiao Orefield. Data source: Neoproterozoic granites in the Jiangnan domain (after Wang XL et al., 2013; Zhang SB and Zheng YF, 2013); Douling complex in the north margin of the Yangtze block (after Hu J et al., 2013); Kongling Group (after Zhang SB et al., 2006; Guo JL et al., 2014).

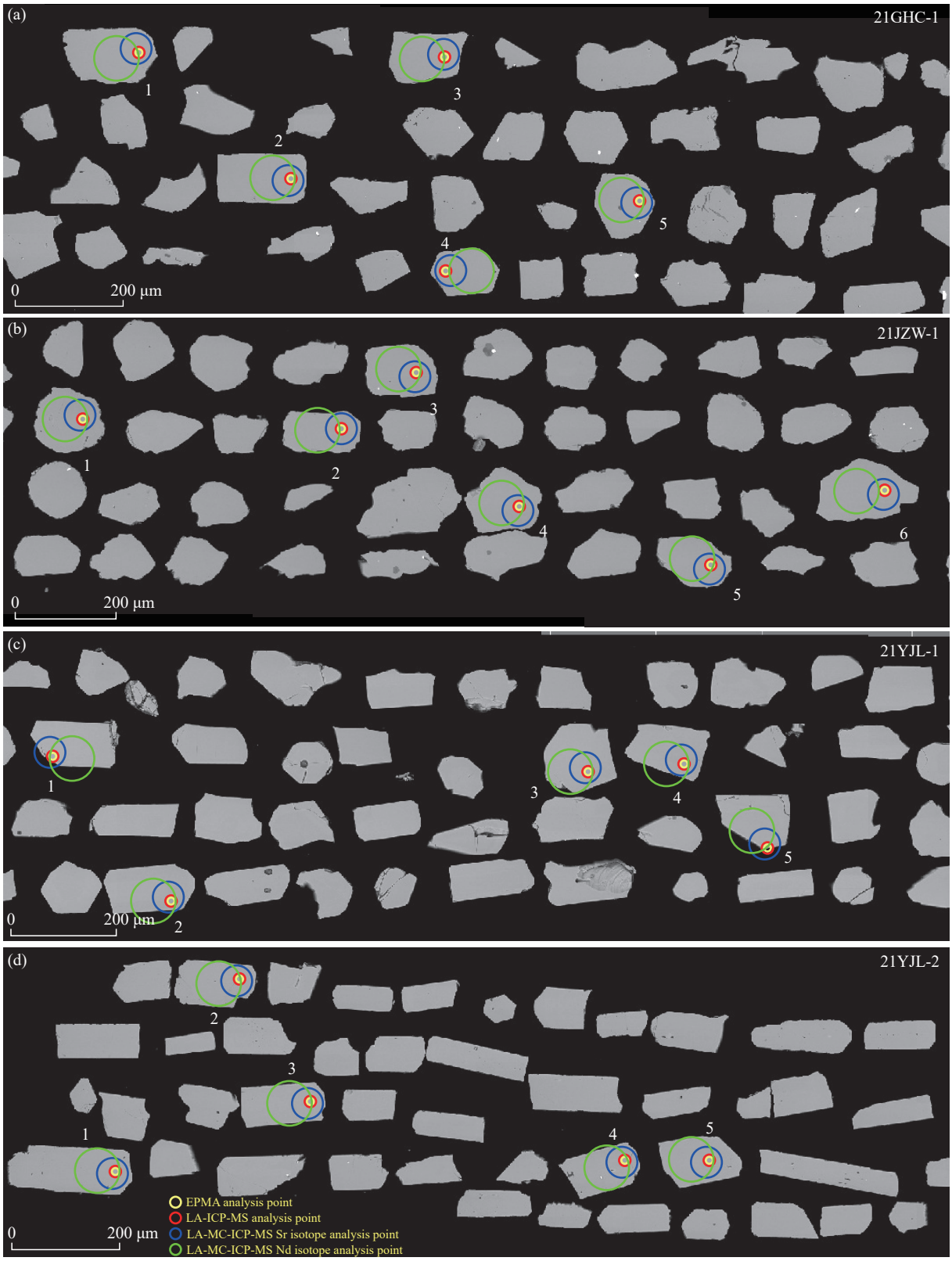


Fig. 6. BSE images of apatite in the Guihuachong (a), Jinziwei (b) and Yaojialing (c,d) intrusions in the Shatanjiao Orefield.

5. Discussion

5.1. Adakitic or non-adakitic affinity for the ore-related granodioritic rocks and ore-barren granite porphyry: An apatite geochemistry perspective

Adakites characteristically originate from the partial melting of young, subducted oceanic crust at relatively deep levels within the subduction zone (> 33 km). Amphibole (± garnet) is stable within this depth range, while plagioclase is suppressed (Müntener O et al., 2001). This selective melting process generates residual melts enriched in Sr and depleted in Y and Yb, reflecting the compatibility of these

elements in amphibole and garnet, respectively. The suppression of plagioclase in the source region further contributes to the adakitic signature, resulting in melts that lack pronounced negative Eu anomalies, as both Sr and Eu are readily incorporated into plagioclase. While sharing characteristic geochemical signatures with adakites, adakitic rocks exhibit distinct formation conditions. Despite these differences, both adakites and adakitic rocks are widely recognized for their close association with porphyry Cu deposits (Sajona FG and Maury RC, 1998; Wang Q et al., 2006; Sun WD et al., 2010; Richards JP, 2011; Sun WD et al., 2012, 2015; Deng JH et al., 2016; Deng JH et al., 2017). The identification of adakites and adakitic rocks holds significant implications for understanding porphyry-skarn systems.

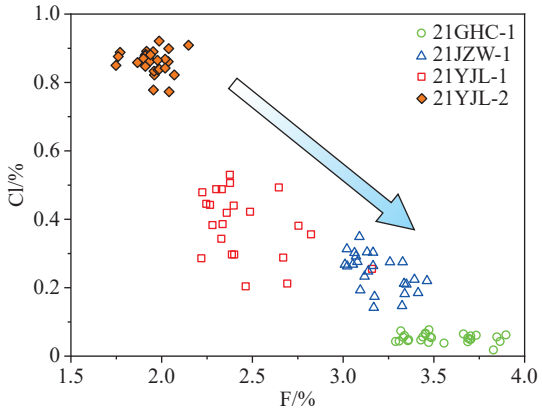


Fig. 7. Plots of F *vs.* Cl of apatite in the Shatanjiao Orefield.

However, the pervasive alteration frequently affecting ore-related rocks often hinders the reliable identification of adakitic affinities based solely on whole-rock geochemistry. Apatite, a ubiquitous accessory mineral in igneous rocks, exhibits compatibility with both Sr and rare earth elements (REEs). Consequently, the geochemical signatures of apatite provide valuable insights into the nature of their parental magmas and can be utilized to identify adakitic affinities (Pan LC et al., 2016; Sun WD et al., 2019; Bruand E et al., 2020; Nathwani CL et al., 2020). Specifically, apatite crystallized from adakitic magmas is expected to inherit characteristically high Sr/Y and $(La/Yb)_N$ ratios, as well as elevated δEu values, reflecting the distinctive geochemical features of their parental melts. Previous studies have established the adakitic nature of ore-related dioritic rocks within the Tongling ore-cluster region (Wang Q et al., 2003; Xie JC et al., 2012a; Wang SW et al., 2015; Xie JC et al., 2018a). Given the similar sampling location and methodology employed by Wang Y et al. (2022b) and the present study, this study classify the granodiorites (porphyries) from the Shatanjiao Orefield as adakitic rocks. This classification is based on their apatite compositions, which exhibit elevated Sr/Y and $(La/Yb)_N$ values, coupled with low Y and Yb contents (Fig. 10). Conversely, the granite porphyry displays distinct apatite characteristics, including lower Sr/Y and $(La/Yb)_N$ values and notably higher Y and Yb contents, consistent with a non-adakitic classification. The δEu values of apatite further support this distinction. The granite porphyry (21YJL-2) exhibits lower δEu values compared to co-eval adakitic rocks,

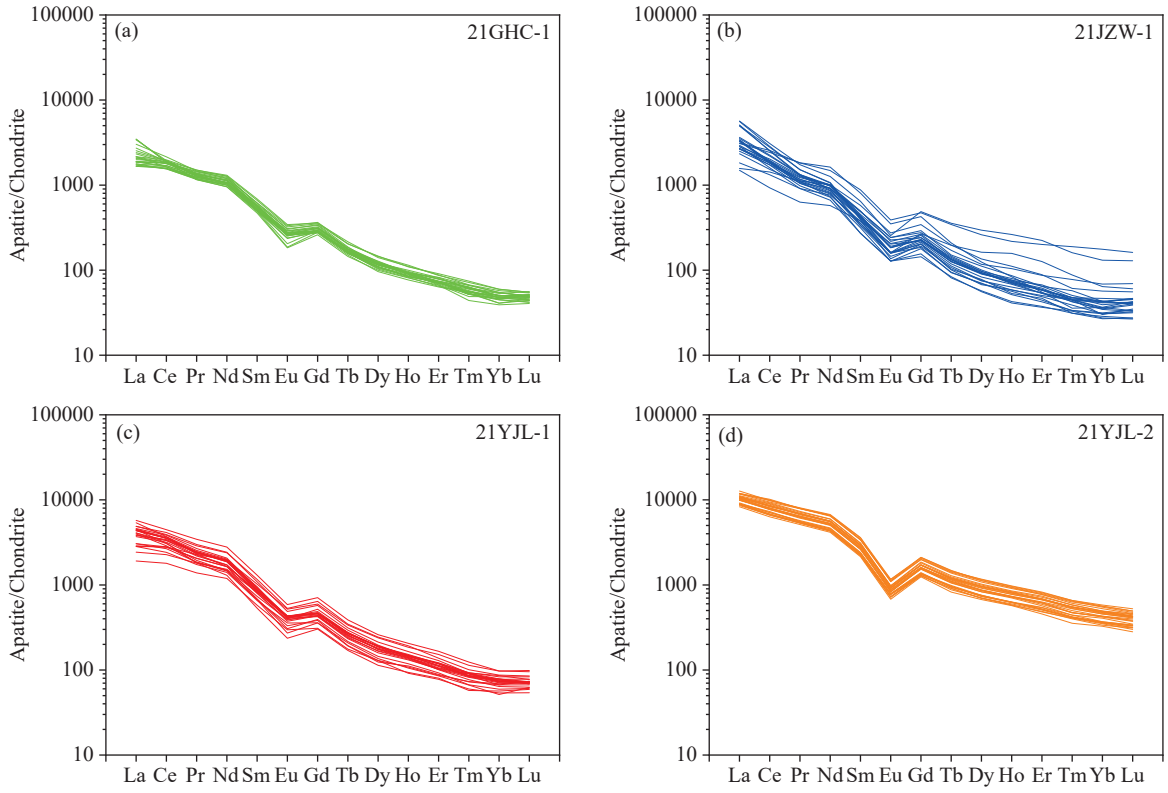


Fig. 8. Chondrite-normalized REE patterns of apatite in the Guihuachong (a), Jinziwei (b) and Yaojialing (c,d) intrusions in the Shatanjiao Orefield. Chondrite REE abundances refer to Sun SS and McDonough WF (1989).

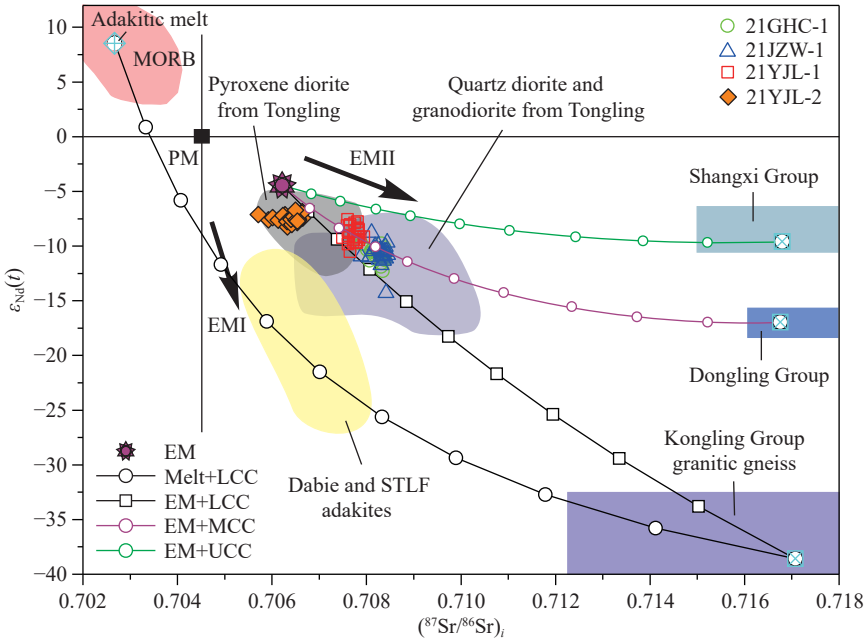


Fig. 9. $^{87}Sr/^{86}Sr$ *vs.* $\varepsilon_{Nd}(t)$ diagram of apatite in the Shatanjiao Orefield. The field of the granitic gneiss of the Kongling Group from Chen JF et al. (2001), the fields of Dabie and STLF adakites from Liu SA et al. (2010), the fields of MORB and marine sediments from Hofmann AW (2014), and the fields of pyroxene diorite, quartz diorite and granodiorite of Tongling from Wang Y et al. (2022b).

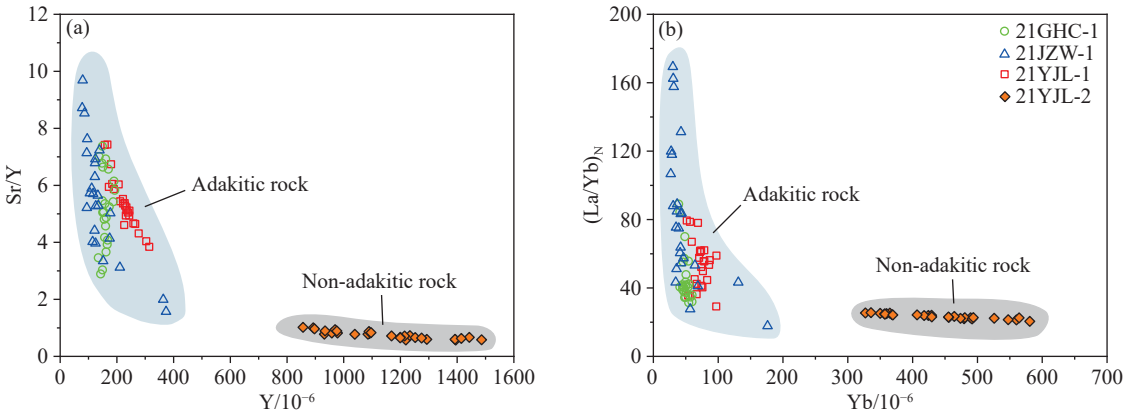


Fig. 10. a–Y *vs.* Sr/Y and b–Yb_N *vs.* $(La/Yb)_N$ discrimination diagrams of apatite in the Shatanjiao Orefield.

spanning the non-adakitic field defined by Pan LC et al. (2016) and highlighting the variability of apatite compositions in non-adakitic rocks across different geological settings (Fig. 11).

5.2. Magma source of ore-related granodioritic rocks and ore-barren granite porphyry

Apatites from three ore-related granodiorites (porphyries) exhibit similar initial $^{87}Sr/^{86}Sr$ ratios (0.707501–0.708457) and $\varepsilon_{Nd}(t)$ values (−14.3 to −7.6; Fig. 9). Together with the similar zircon Lu-Hf isotopic compositions (−14.6 to −7.3; Fig. 5) and zircon U-Pb ages (139.3 Ma to 142.5 Ma) of these ore-related granodiorites, it is suggested a common magmatic source for these intrusions. Although the ore-barren granite porphyry is spatially proximal to the three aforementioned intrusions (Fig. 2), its apatite Sr-Nd isotopic composition ($^{87}Sr/^{86}Sr$: 0.705718 to 0.706657; $\varepsilon_{Nd}(t)$: −8.2 to −6.7) and

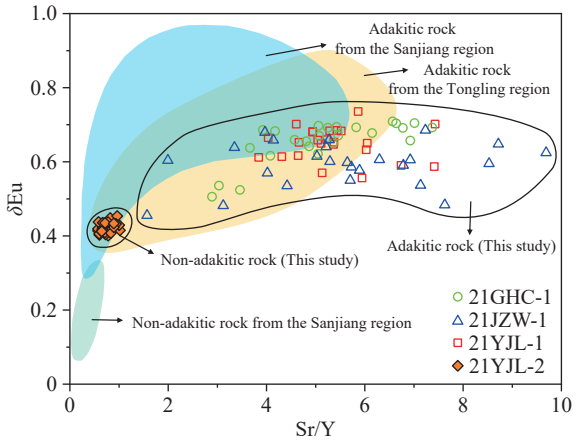


Fig. 11. Sr/Y *vs.* δEu diagram of apatite in the Shatanjiao Orefield. Data from the Sanjiang region, and Tongling region refer to Pan LC et al. (2016) and Wang Y et al. (2019), respectively.

zircon Hf isotopic composition (−6.6 to −4.6) differ significantly, indicating a distinct magmatic source in the three ore-related intrusions.

The genesis of ore-related adakitic rocks within the MLYRB has been a subject of ongoing debate, with several competing models proposed to explain their origin. These models include: (1) Derivation from the interaction of thickened or delaminated lower crust with mantle peridotites (Zhang Q et al., 2001; Xu JF et al., 2002; Wang Q et al., 2004, 2006, 2007b); (2) fractional crystallization of mantle-derived basaltic magma (Li et al., 2009); (3) mixing of mantle-derived and crust-derived magmas (Xu JF et al., 2004; Xu YM et al., 2014); and (4) partial melting of subducted oceanic crust, potentially accompanied by assimilation of enriched components from the lithospheric mantle and/or crustal materials (Liu SA et al., 2010; Xie JC et al., 2018b; Wang Y et al., 2022a, b). However, several lines of evidence argue against a purely crustal origin for the adakitic rocks in the Shatanjiao Orefield. Their Sr-Nd isotopic compositions are distinct from those of adakitic rocks in the Dabie orogenic belt and those associated with the Tancheng-Lujiang Fault (STLF), which are widely attributed to lower crustal melting (Liu SA et al., 2010). They also differ from the Kongling gneiss, representative of the Upper Yangtze crust (Chen JF et al., 2001). Furthermore, zircon Lu-Hf isotopic compositions from this study plot between the evolutionary trends of Archean crustal endmembers (Kongling Group and Douling Complex) and Proterozoic crust, inconsistent with an origin solely from ancient crustal sources (Fig. 5). While typical adakites generated by slab melting exhibit depleted Sr-Nd isotopic signatures ($^{87}Sr/^{86}Sr < 0.7040$, $\varepsilon_{Nd}(t) > 0$) (Defant and Drummond, 1990), the ore-related adakitic rocks in this study display significantly enriched Sr-Nd isotopic compositions. This enrichment, coupled with the presence of ancient zircon grains, points toward the involvement of crustal components in their petrogenesis (Yang XY et al., 2011; Tang M et al., 2012; Yang W and Zhang HF, 2012; Yang YZ et al., 2014; Yan J et al., 2015). Moreover, the analyzed apatite compositions are comparable to those of quartz diorites and granodiorites from the Tongling region and occupy an intermediate isotopic space between MORB and marine sediments (Fig. 9). Collectively, these geochemical and isotopic data suggest that the ore-related adakitic rocks of the Shatanjiao Orefield originated primarily from the partial melting of subducted oceanic crust, which is similar to these typical adakitic rocks (Richards JP and Kerrich R, 2007; Richards JP, 2011). However, significant assimilation of Yangtze crustal material during magma ascent played a crucial role in modifying their geochemical and isotopic signatures. The Sr-Nd isotopic compositions of apatite from the ore-barren granite porphyry exhibit similarities to those of pyroxene diorites in the region, which are interpreted to be originated from the partial melting of a lithospheric mantle source that underwent metasomatism by slab-derived melts (Xie JC et al., 2012b; Xie JC et al., 2018b; Wang Y et al., 2022b). This interpretation is further supported by the more depleted Hf isotopic signatures than ore-related rocks observed in zircon of the granite porphyry. It was proposed that copper and gold concentrations in the oceanic crust are about two times higher than those in the continental crust, resulting in oceanic crust-derived melts containing more copper and gold than those in continental crust-derived melts (Sun WD et al., 2012). Therefore, ore-related granodioritic rocks are more favorable for Cu-Au mineralization than ore-barren granite porphyry.

5.3. Oxygen fugacity: A controlling factor for the Cu-Au mineralization

The multi-valent elements in apatite, such as Ce, Eu, Ga, and Mn, can be used to estimate the oxygen fugacity of magma (Sha LK and Chappell BW, 1999; Cao MJ et al., 2012; Pan LC et al., 2016; Xie JC et al., 2018a; Xing K et al., 2020; Bromiley, GD 2021; Zhang SY et al., 2021). Apatite preferentially incorporates Ce^{3+}, Eu^{3+}, Ga^{2+}, and Mn^{2+} due to their ability to substitute for Ca^{2+} within the apatite crystal structure, while sulfur, in its +6 valence state, substitutes for P within the apatite structure (Sha and Chappell, 1999; Belousova et al., 2002; Pan and Fleet, 2002). In addition, elevated oxygen fugacity conditions promote the increase of Ce^{4+}, Eu^{3+}, Ga^{3+}, and Mn^{4+} concentrations, while concomitantly decreasing the concentrations of Ce^{3+}, Eu^{2+}, Ga^{2+}, and Mn^{2+}. However, it is essential to consider that factors beyond redox changes, such as mineral fractionation, can significantly influence the trace element compositions of evolving magmas (Belousova EA et al., 2002; Chu MF et al., 2009). Therefore, relying solely on the variation of a single trace element in apatite to reflect changes in magma oxidation state may lead to ambiguous or erroneous interpretations. Semi-quantitative estimation of oxygen fugacity is more effectively achieved using binary diagrams of two multivalent elements. Analysis reveals a negative correlation between δCe and δEu in apatite, while Ga, Mn, and δEu exhibit a positive correlation. These findings suggest that oxygen fugacity plays a crucial role in regulating the concentrations of these elements within the magma system. As depicted in Figs. 12a–c, three granodiorite (porphyry) samples formed under comparable conditions characterized by higher oxygen fugacities than the ore-barren granite porphyry.

Zircon is one of the common minerals in magmatic rocks and is regarded as a reliable redox indicator (e.g., Burnham AD and Berry AJ, 2012; Smythe DJ and Brenan JM, 2016; Zhang CC et al., 2017). The oxygen fugacity values estimated from zircon trace element of ore-related rocks are from ΔFMQ+0.59 to ΔFMQ+3.41 with the average value of ΔFMQ+2.00 at 760°C, which is distinctly higher than that of ore-barren rock (ΔFMQ+1.22 to ΔFMQ+1.75, with the average value of ΔFMQ+1.43 at 962°C). Besides, the Eu/Eu* values of two types of rocks are from 0.50 to 0.88 with an average value of 0.64 and 0.64 to 0.55 with an average value of 0.39, respectively (Fig. 12d). Thus, the evidence of zircon trace element further prove the ore-related rocks were formed

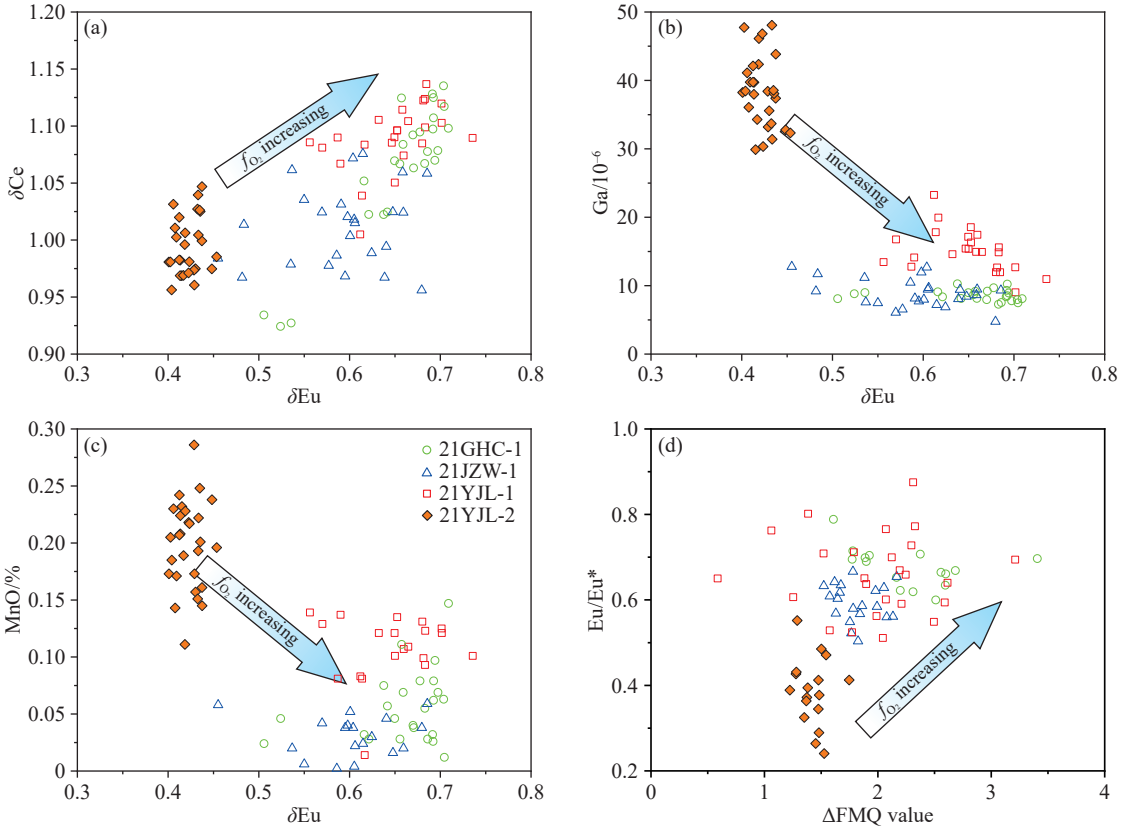


Fig. 12. a–δEu *vs*. δCe, b–Ga, and c–MnO diagram of apatite and d–Eu/Eu* *vs*. ΔFMQ of zircon in the Shatanjiao Orefield.

on a more oxidized environment.

The genesis of high oxygen fugacity (f_{O_2}) igneous rocks associated with Cu-Au mineralization is widely attributed to the partial melting of subducted oceanic crust, since high f_{O_2} will promote the release of copper and gold during melting (Sun WD et al., 2010; Sun WD et al., 2012; Deng JH et al., 2019; Xu JF and Chen SS, 2023). This process is believed to produce magmas enriched in water, volatiles, and metals. Elevated f_{O_2} conditions further enhance metal extraction, resulting in Cu-Au-enriched magmas conducive to mineralization (Zhang H et al., 2013; Zhang CC et al., 2017; Alex A and Zajacz Z, 2022). Modeling studies indicated that the Cu content of slab melts reaches a maximum of >500× 10^{-6} at about 15% partial melting and ΔFMQ > +2, which is beneficial to the Cu-Au mineralization (Sun WD et al., 2017). Conversely, partial melting of the lower crust typically yields magmas characterized by low f_{O_2} and depleted concentrations of water and metals, which will prejudice the remobilization of Cu-Au and mineralization (Sun WD et al., 2010). In addition, the Cu-Au mineralization-related magmatic rocks in the MLYRB were mainly emplaced within the range of 152–124 Ma and were related to the subduction of the Paleo-Pacific plate (Deng JH et al., 2016; Jiang XY et al., 2020; Wang Y et al., 2022b). The ore-related magmatic rocks in the MLYRB are characterized by high oxygen fugacity, which is regarded as one of the key factors in controlling the regional Cu-Au mineralization (Li C et al., 2017; Xie JC et al., 2018b; Jiang XY et al., 2020; Wang Y et al., 2022b; Cao JY et al., 2022). In the present study, ore-related granodiorite (porphyry) and ore-barren granite porphyry show distinct oxidation states with average ΔFMQ + 2.0 and ΔFMQ + 1.43, respectively, further confirming that oxygen fugacity is one of the key factors in the Cu-Au mineralization.

5.4. Volatiles: implications to regional Cu-Au mineralization

Volatiles, such as F and Cl in apatite, have important significance for porphyry-skarn Cu polymetallic ore-related systems (Belousova EA et al., 2002; Imai A, 2004; Jiang XY et al., 2020; Zhang SY et al., 2021). The Cl contents of apatite can be used to estimate the Cl contents in the initial magma, as they do not decrease during fractional crystallization and are not susceptible to subsolidus halogen exchange (Sha LK and Chappell BW, 1999). Generally, fluids/melts derived from subducted slabs have relatively high Cl contents (Kendrick MA et al., 2011; Reynard B, 2013), whereas continental crust is rich in F since sediment loses more Cl than F during weathering. Chalcophile elements, such as Cu, Au, and Zn, are more sensitive to Cl than F because they are transported in hydrothermal fluids in the form of complexes with HS^- or Cl^- ions (Mavrogenes JA et al., 2002; Hack AC and Mavrogenes JA, 2006). Some authors have demonstrated that apatite of ore-related rocks commonly contains high Cl and S contents in many porphyry-type Cu polymetallic deposits (Xie JC et al., 2018b; Zhang SY et al., 2021). In this study, apatite in the ore-related intrusions has relatively lower Cl and higher F contents (Cl: 0.02%–0.53%, average 0.22%; F: 2.22%–3.90%, average 3.10%) than the ore-barren granite

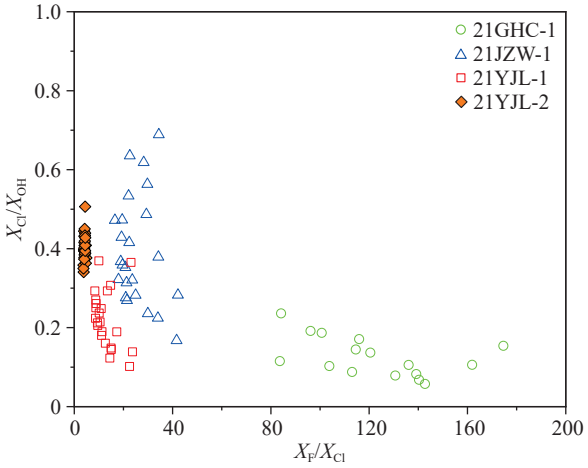


Fig. 13. X_F/X_{Cl} *vs.* X_{Cl}/X_{OH} diagram of apatite in the Shatanjiao Orefield.

porphyry (Cl: 0.77%–0.92%, average 0.92%; F: 1.75%–2.15%, average 1.95%).

Magmatic water concentration exerts a critical control on Cu-Au mineralization systems, as elevated water contents promote high-pressure aqueous phase saturation in magmas, enhancing the efficient extraction and transport of ore metals (Kelser SE and Wilkinson BH, 2009; Sillitoe RH, 2010). X_F/X_{Cl} and X_{Cl}/X_{OH} ratios of the ore-related rocks show a negative correlation which was consistent with water-saturated evolution, indicating a water-enriched melt (Fig. 13; Stock MJ et al., 2016, 2018). Since Cl partitions preferentially (to F) into fluids, the water fluid exsolution process in a water-saturated melt will result in higher X_F/X_{Cl} and lower X_{Cl}/X_{OH} (Lormand C et al., 2024). In terms of the ore-barren rocks, no correlation was identified between X_F/X_{Cl} and X_{Cl}/X_{OH}, indicating a water-unsaturated melt (Fig. 13). Considering the high Cl contents in these ore-barren rocks, it might be indicated that these apatite might be crystallized from a Cl-rich magma chamber (Lormand C et al., 2024). Thus, the lower Cl contents of apatite in ore-related rocks, crystallized from a water-saturated melt, do not indicate a low Cl budget for these ore-related melts (Huang WT et al., 2024). Therefore, the high water content might also emerge as one of the critical factors governing the regional Cu-Au mineralization potential of magmatic rocks within the Shatanjiao ore field.

6. Conclusions

(i) The ore-related granodiorites with ages of 139.3 Ma to 142.5 Ma exhibit adakitic affinities and are characterized by lower zircon $\varepsilon_{Hf}(t)$ values of −14.6 to −7.3 and apatite $\varepsilon_{Nd}(t)$ values of −14.3 to −7.6, consistent with derivation from partial melting of subducted oceanic crust with assimilation of Yangtze crustal materials and favoring the Cu-Au mineralization. In contrast, the ore-barren granite porphyry with an age of 121.0 ± 2.8 Ma originates from lithospheric mantle sources with relatively higher zircon $\varepsilon_{Hf}(t)$ values of −8.6 to −4.6 and apatite $\varepsilon_{Nd}(t)$ values of −8.2 to −6.7.

(ii) The ore-related granodiorites record elevated oxygen fugacity conditions (ΔFMQ > +2), favoring the mobilization of Cu and Au during partial melting. By comparison, the ore-barren granite porphyry shows lower f_{O_2} values (ΔFMQ = +1.43), which suppressed Cu-Au mineralization potential.

(iii) Distinct apatite X_F/X_{Cl} and X_{Cl}/X_{OH} correlations distinguish the two magma types: the ore-related granodiorites reflect water-saturated magmas, while the ore-barren porphyries correspond to water-unsaturated systems.

CRediT authorship contribution statement

Yu Wang finished the original draft and data analyses. Jing-ya Cao presented the idea. Yu Wang and Muhammad Hafeezc carried out the experiment. Yu Wang, Sheng-xiong Yang and Xiao-yong Yang took part in the field investigation. Majid Ghasemi Sianid and Asghar Dolatid took part in the discussion and English editing. All authors discussed the results and contributed to the final manuscript.

Declaration of competing interest

The authors declare no conflicts of interest.

Acknowledgments

This study was supported by the National Natural Science Foundation of China (42472117), the China Geological Survey Project (DD20230040), the Natural Science Foundation of Anhui Province (2108085MD133), and the PI Project of Southern Marine Science and Engineering Guangdong Laboratory (Guangzhou) (GML2020GD0802). The authors also appreciate the insightful comments and suggestions from the anonymous reviewers and the editors from *China Geology*.

Supplementary dataset

Supplementary data (Tables S1–S4) to this article can be found online at doi: 10.31035/cg2024105.

References

Alex A, Zajacz Z. 2022. The solubility of Cu, Ag and Au in magmatic sulfur-bearing fluids as a function of oxygen fugacity. Geochimica et Cosmochimica Acta, 330, 93–115. doi: 10.1016/j.gca.2022.03.036.

Ballard JR, Palin JM, Campbell IH. 2002. Relative oxidation states of magmas inferred from Ce(IV)/Ce(III) in zircon: Application to porphyry copper deposits of northern Chile. Contributions to Mineralogy and Petrology, 144(3), 347–364. doi: 10.1007/s00410-002-0402-5.

Belousova EA, Griffin WL, O'Reilly SY, Fisher NI. 2002. Apatite as an indicator mineral for mineral exploration: Trace-element compositions and their relationship to host rock type. Journal of Geochemical Exploration, 76(1), 45–69. doi: 10.1016/s0375-6742(02)00204-2.

Bromiley GD. 2021. Do concentrations of Mn, Eu and Ce in apatite reliably record oxygen fugacity in magmas? Lithos, 384–385, 105900. doi: 10.1016/j.lithos.2020.105900.

Bruand E, Fowler M, Storey C, Darling J. 2017. Apatite trace element and isotope applications to petrogenesis and provenance. American

Mineralogist, 102(1), 75–84. doi: 10.2138/am-2017-5744.
Bruand E, Fowler M, Storey C, Laurent O, Antoine C, Guitreau M, Heilimo E, Nebel O. 2020. Accessory mineral constraints on crustal evolution: Elemental fingerprints for magma discrimination. Geochemical Perspectives Letters, 7–12. doi: 10.7185/geochemlet.2006.
Burnham AD, Berry AJ. 2012. An experimental study of trace element partitioning between zircon and melt as a function of oxygen fugacity. Geochimica et Cosmochimica Acta, 95, 196–212. doi: 10.1016/j.gca.2012.07.034.
Cao JY, Li H, Yang XY, Tamehe LS, Esmaeili R. 2022. Multi-stage magma evolution recorded by apatite and zircon of adakite-like rocks: A case study from the Shatanjiao intrusion, Tongling region, Eastern China. American Mineralogist, 107(2), 178–189. doi: 10.2138/am-2021-7871.
Cao JY, Yang XY, Yang SX, Zhong C, Wang Y. 2023. Records of apatite for multiple injections of magmas in adakitic plutons: A case study of Mesozoic plutons in the Shatanjiao region of the Tongling ore cluster, South China. Journal of Asian Earth Sciences, 242, 105507. doi: 10.1016/j.jseaes.2022.105507.
Cao MJ, Li GM, Qin KZ, Seitmuratova EY, Liu YS. 2012. Major and trace element characteristics of apatites in granitoids from central Kazakhstan: Implications for petrogenesis and mineralization. Resource Geology, 62(1), 63–83. doi: 10.1111/j.1751-3928.2011.00180.x.
Castillo PR, Janney PE, Solidum RU. 1999. Petrology and geochemistry of Camiguin Island, southern Philippines: Insights to the source of adakites and other lavas in a complex arc setting. Contributions to Mineralogy and Petrology, 134(1), 33–51. doi: 10.1007/s004100050467.
Chang YF, Liu XP, Wu YC. 1991. The Copper–iron Belt of the Middle and Lower Reaches of the Changjiang River. Beijing, Geological Publishing House, 379 (in Chinese with English abstract).
Chen JF, Yan J, Xie Z, Xu X, Xing F. 2001. Nd and Sr isotopic compositions of igneous rocks from the Lower Yangtze region in Eastern China: Constraints on sources. Physics and Chemistry of the Earth, Part A: Solid Earth and Geodesy, 26(9–10), 719–731. doi: 10.1016/s1464-1895(01)00122-3.
Chu MF, Wang KL, Griffin WL, Chung SL, O'Reilly SY, Pearson NJ, Iizuka Y. 2009. Apatite composition: Tracing petrogenetic processes in transhimalayan granitoids. Journal of Petrology, 50(10), 1829–1855. doi: 10.1093/petrology/egp054.
Chung SL, Liu DY, Ji JQ, Chu MF, Lee HY, Wen DJ, Lo CH, Lee TY, Qian Q, Zhang Q. 2003. Adakites from continental collision zones: Melting of thickened lower crust beneath southern Tibet. Geology, 31(11), 1021. doi: 10.1130/g19796.1.
Defant MJ, Drummond MS. 1990. Derivation of some modern arc magmas by melting of young subducted lithosphere. Nature, 347(6294), 662–665. doi: 10.1038/347662a0.
Defant MJ, Kepezhinskas P. 2001. Evidence suggests slab melting in arc magmas. Eos, Transactions American Geophysical Union, 82(6), 65–69. doi: 10.1029/01eo00038.
Deng JH, Yang XY, Li S, Gu HL, Mastoi AS, Sun WD. 2016. Partial melting of subducted paleo-Pacific plate during the Early Cretaceous: Constraint from adakitic rocks in the Shaxi porphyry Cu–Au deposit, Lower Yangtze River Belt. Lithos, 262, 651–667. doi: 10.1016/j.lithos.2016.07.039.
Deng JH, Yang XY, Qi HS, Zhang ZF, Mastoi AS, Sun WD. 2017. Early Cretaceous high-Mg adakites associated with Cu-Au mineralization in the Cebu Island, Central Philippines: Implication for partial melting of the paleo-Pacific Plate. Ore Geology Reviews, 88, 251–269. doi: 10.1016/j.oregeorev.2017.05.006.
Deng JH, Yang XY, Qi HS, Zhang ZF, Mastoi AS, Berador AEG, Sun WD. 2019. Early Cretaceous adakite from the Atlas porphyry Cu-Au deposit in Cebu Island, Central Philippines: Partial melting of subducted oceanic crust. Ore Geology Reviews, 110, 102937. doi: 10.1016/j.oregeorev.2019.102937.
Gao S, Rudnick RL, Yuan HL, Liu XM, Liu YS, Xu WL, Ling WL, Ayers J, Wang XC, Wang QH. 2004. Recycling lower continental crust in the North China Craton. Nature, 432(7019), 892–897. doi: 10.1038/nature03162.
Guo JL, Gao S, Wu YB, Li M, Chen K, Hu ZC, Liang ZW, Liu YS, Zhou L, Zong KQ, Zhang W, Chen HH. 2014. 3.45 Ga granitic gneisses from the Yangtze craton, South China: Implications for early Archean crustal growth. Precambrian Research, 242, 82–95. doi: 10.1016/j.precamres.2013.12.018.
Ferry JM, Watson EB. 2007. New thermodynamic models and revised calibrations for the Ti-in-zircon and Zr-in-rutile thermometers. Contributions to Mineralogy and Petrology, 154(4), 429–437. doi: 10.1007/s00410-007-0201-0.
Hack AC, Mavrogenes JA. 2006. A synthetic fluid inclusion study of copper solubility in hydrothermal brines from 525 to 725°C and 0.3 to 1.7GPa. Geochimica et Cosmochimica Acta, 70(15), 3970–3985. doi: 10.1016/j.gca.2006.04.035.
Hofmann AW. 2014. Sampling mantle heterogeneity through oceanic basalts: Isotopes and trace elements. Treatise on Geochemistry. Amsterdam: Elsevier, 67–101. doi: 10.1016/b978-0-08-095975-7.00203-5.
Hoskin PWO. 2003. The composition of zircon and igneous and metamorphic petrogenesis. Reviews in Mineralogy and Geochemistry, 53(1), 27–62. doi: 10.2113/0530027.
Hu J, Liu XC, Chen LY, Qu W, Li HK, Geng JZ. 2013. A ~2.5 Ga magmatic event at the northern margin of the Yangtze craton: Evidence from U-Pb dating and Hf isotope analysis of zircons from the Douling Complex in the South Qinling orogen. Chinese Science Bulletin, 58(28), 3564–3579. doi: 10.1007/s11434-013-5904-1.
Huang WM, Wu CL, Gao D, Wu D, Liu CY, Zeng Q. 2019. Petrogenesis and tectonic implications of the intermediate-acid plutons in Shatanjiao ore-field, Tongling, Anhui. Geology in China, 46(4), 861–877 (in Chinese with English abstract). doi: 10.12029/gc20190416.
Huang WT, Stock MJ, Xia XP, Sun XM, Cui ZX, Ouyang LY, Zhang J, Chen XL, Zheng Y, Liang HY. 2024. Determining the impact of magma water contents on porphyry Cu fertility: Constraints from hydrous and nominally anhydrous mineral analyses. GSA Bulletin, 136(1-2), 673–688. doi: 10.1130/B37180.1.
Imai A. 2004. Variation of Cl and SO_3 contents of microphenocrystic apatite in intermediate to silicic igneous rocks of Cenozoic Japanese Island arcs: Implications for porphyry Cu metallogenesis in the western Pacific Island arcs. Resource Geology, 54(3), 357–372. doi: 10.1111/j.1751-3928.2004.tb00211.x.
Jiang XY, Deng JH, Luo JC, Zhang LP, Luo ZB, Yan HB, Sun WD. 2020. Petrogenesis of Early Cretaceous adakites in Tongguanshan Cu–Au polymetallic deposit, Tongling region, Eastern China. Ore Geology Reviews, 126, 103717. doi: 10.1016/j.oregeorev.2020.103717.
Kesler SE, Wilkinson BH. 2009. Resources of gold in Phanerozoic epithermal deposits. Economic Geology, 104(5): 623–633. doi: 10.2113/gsecongeo.104.5.623.
Kendrick MA, Scambelluri M, Honda M, Phillips D. 2011. High abundances of noble gas and chlorine delivered to the mantle by serpentinite subduction. Nature Geoscience, 4(11), 807–812. doi: 10.1038/ngeo1270.
Laurent O, Zeh A, Gerdes A, Villaros A, Gros K, Słaby E. 2017. How do granitoid magmas mix with each other? Insights from textures, trace element and Sr–Nd isotopic composition of apatite and titanite from the Matok pluton (South Africa). Contributions to Mineralogy and Petrology, 172(9), 80. doi: 10.1007/s00410-017-1398-1.
Li CY, Hao XL, Liu JQ, Ling MX, Ding X, Zhang H, Sun WD. 2017. The formation of Luoboling porphyry Cu–Mo deposit: Constraints from zircon and apatite. Lithos, 272–273, 291–300. doi: 10.1016/j.lithos.2016.12.003.
Li JW, Zhao XF, Zhou MF, Ma CQ, de Souza ZS, Vasconcelos P. 2009. Late Mesozoic magmatism from the Daye region, Eastern China: U–Pb ages, petrogenesis, and geodynamic implications. Contributions to Mineralogy and Petrology, 157(3), 383–409. doi: 10.1007/s00410-008-0341-x.
Li WR, Costa F. 2020. A thermodynamic model for F-Cl-OH

partitioning between silicate melts and apatite including non-ideal mixing with application to constraining melt volatile budgets. Geochimica et Cosmochimica Acta, 269, 203–222. doi: 10.1016/j.gca.2019.10.035.

Liu SA, Li SG, He YS, Huang F. 2010. Geochemical contrasts between Early Cretaceous ore-bearing and ore-barren high-Mg adakites in central-eastern China: Implications for petrogenesis and Cu–Au mineralization. Geochimica et Cosmochimica Acta, 74(24), 7160–7178. doi: 10.1016/j.gca.2010.09.003.

Liu YS, Gao S, Hu ZC, Gao CG, Zong KQ, Wang DB. 2010. Continental and oceanic crust recycling-induced melt-peridotite interactions in the Trans-North China Orogen: U-Pb dating, Hf isotopes and trace elements in zircons from mantle xenoliths. Journal of Petrology, 51(1–2), 537–571. doi: 10.1093/petrology/egp082.

Liu YS, Hu ZC, Gao S, Günther D, Xu J, Gao CG, Chen HH. 2008. *In situ* analysis of major and trace elements of anhydrous minerals by LA-ICP-MS without applying an internal standard. Chemical Geology, 257(1–2), 34–43. doi: 10.1016/j.chemgeo.2008.08.004.

Lormand C, Humphreys MCS, Colby DJ, Coumans JP, Chelle-Michou C, Li WR. 2024. Volatile budgets and evolution in porphyry-related magma systems, determined using apatite. Lithos, 480–481, 107623. doi: 10.1016/j.lithos.2024.107623.

Loucks RR, Fiorentini ML, Henríquez GJ. 2020. New magmatic oxybarometer using trace elements in zircon. Journal of Petrology, 61(3), egaa034. doi: 10.1093/petrology/egaa034.

Ma Y, Jiang S, Frimmel HE. 2023. Apatite records metamorphic and hydrothermal fluid evolution at the large Shuangqishan orogenic gold deposit, SE China. GSA Bulletin, 135(11–12), 3005–3023. doi: 10.1130/B36642.1.

Mavrogenes JA, Berry AJ, Newville M, Sutton SR. 2002. Copper speciation in vapor-phase fluid inclusions from the Mole Granite, Australia. American Mineralogist, 87(10), 1360–1364. doi: 10.2138/am-2002-1011.

Miles AJ, Graham CM, Hawkesworth CJ, Gillespie MR, Hinton RW, Bromiley GD. 2014. Apatite: A new redox proxy for silicic magmas? Geochimica et Cosmochimica Acta, 132, 101–119. doi: 10.1016/j.gca.2014.01.040.

Müntener O, Kelemen PB, Grove TL. 2001. The role of H_2O during crystallization of primitive arc magmas under uppermost mantle conditions and genesis of igneous pyroxenites: An experimental study. Contributions to Mineralogy and Petrology, 141(6), 643–658. doi: 10.1007/s004100100266.

Nathwani CL, Loader MA, Wilkinson JJ, Buret Y, Sievwright RH, Hollings P. 2020. Multi-stage arc magma evolution recorded by apatite in volcanic rocks. Geology, 48(4), 323–327. doi: 10.1130/g46998.1.

Pan LC, Hu RZ, Wang XS, Bi XW, Zhu JJ, Li CS. 2016. Apatite trace element and halogen compositions as petrogenetic-metallogenic indicators: Examples from four granite plutons in the Sanjiang region, SW China. Lithos, 254–255, 118–130. doi: 10.1016/j.lithos.2016.03.010.

Pan YM, Dong P. 1999. The Lower Changjiang (Yangzi/Yangtze River) metallogenic belt, east Central China: Intrusion- and wall rock-hosted Cu–Fe–Au, Mo, Zn, Pb, Ag deposits. Ore Geology Reviews, 15(4), 177–242. doi: 10.1016/s0169-1368(99)00022-0.

Pan YM, Fleet ME. 2002. Compositions of the apatite-group minerals: Substitution mechanisms and controlling factors. Phosphates: Geochemical, Geobiological, and Materials Importance, 48, 13–49.

Reynard B. 2013. Serpentine in active subduction zones. Lithos, 178, 171–185. doi: 10.1016/j.lithos.2012.10.012.

Richards JP. 2011. High Sr/y arc magmas and porphyry Cu Mo Au deposits: Just add water. Economic Geology, 106(7), 1075–1081. doi: 10.2113/econgeo.106.7.1075.

Richards JP, Kerrich R. 2007. Special paper: Adakite-like rocks: Their diverse origins and questionable role in metallogenesis. Economic Geology, 102(4), 537–576. doi: 10.2113/gsecongeo.102.4.537.

Sajona FG, Maury RC. 1998. Association of adakites with gold and copper mineralization in the Philippines. Comptes Rendus de L' Académie Des Sciences - Series IIA - Earth and Planetary Science, 326(1), 27–34. doi: 10.1016/s1251-8050(97)83200-4.

Sha LK, Chappell BW. 1999. Apatite chemical composition, determined by electron microprobe and laser-ablation inductively coupled plasma mass spectrometry, as a probe into granite petrogenesis. Geochimica et Cosmochimica Acta, 63(22), 3861–3881. doi: 10.1016/s0016-7037(99)00210-0.

Sillitoe RH. 2010. Porphyry copper systems. Economic Geology, 105: 3–41. doi: 10.2113/gsecongeo.105.1.3.

Smythe DJ, Brenan JM. 2016. Magmatic oxygen fugacity estimated using zircon-melt partitioning of cerium. Earth and Planetary Science Letters, 453, 260–266. doi: 10.1016/j.epsl.2016.08.013.

Stock MJ, Humphreys MCS, Smith VC, Isaia R, Pyle DM. 2016. Late-stage volatile saturation as a potential trigger for explosive volcanic eruptions. Nature Geoscience, 9(3), 249–254. doi: 10.1038/ngeo2639.

Stock MJ, Humphreys MCS, Smith VC, Isaia R, Brooker RA, Pyle DM. 2018. Tracking volatile behaviour in sub-volcanic plumbing systems using apatite and glass: Insights into pre-eruptive processes at Campi flegrei, Italy. Journal of Petrology, 59(12), 2463–2492. doi: 10.1093/petrology/egy020.

Sun SJ, Yang XY, Wang GJ, Sun WD, Zhang H, Li CY, Ding X. 2019. *In situ* elemental and Sr-O isotopic studies on apatite from the Xu-Huai intrusion at the southern margin of the North China Craton: Implications for petrogenesis and metallogeny. Chemical Geology, 510, 200–214. doi: 10.1016/j.chemgeo.2019.02.010.

Sun SS, McDonough WF. 1989. Chemical and isotopic systematics of oceanic basalts: Implications for mantle composition and processes. Geological Society, London, Special Publications, 42(1), 313–345. doi: 10.1144/gsl.sp.1989.042.01.19.

Sun WD, Ling MX, Chung SL, Ding X, Yang XY, Liang HY, Fan WM, Goldfarb R, Yin QZ. 2012. Geochemical constraints on adakites of different origins and copper mineralization. The Journal of Geology, 120(1), 105–120. doi: 10.1086/662736.

Sun WD, Huang RF, Li H, Hu YB, Zhang CC, Sun SJ, Zhang LP, Ding X, Li CY, Zartman RE, Ling MX. 2015. Porphyry deposits and oxidized magmas. Ore Geology Reviews, 65, 97–131. doi: 10.1016/j.oregeorev.2014.09.004.

Sun WD, Ling MX, Yang XY, Fan WM, Ding X, Liang HY. 2010. Ridge subduction and porphyry copper-gold mineralization: An overview. Science China Earth Sciences, 53(4), 475–484. doi: 10.1007/s11430-010-0024-0.

Sun WD, Wang JT, Zhang LP, Zhang CC, Li H, Ling MX, Ding X, Li CY, Liang HY. 2017. The formation of porphyry copper deposits. Acta Geochimica, 36(1), 9–15. doi: 10.1007/s11631-016-0132-4.

Tang M, Wang XL, Xu XS, Zhu C, Cheng T, Yu Y. 2012. Neoproterozoic subducted materials in the generation of Mesozoic Luzong volcanic rocks: Evidence from apatite geochemistry and Hf–Nd isotopic decoupling. Gondwana Research, 21(1), 266–280. doi: 10.1016/j.gr.2011.05.009.

Trail D, Bruce Watson E, Tailby ND. 2012. Ce and Eu anomalies in zircon as proxies for the oxidation state of magmas. Geochimica et Cosmochimica Acta, 97, 70–87. doi: 10.1016/j.gca.2012.08.032.

Wang FY, Ge C, Ning SY, Nie LQ, Zhong GX, White N. 2017. A new approach to LA-ICP-MS mapping and application in geology. Acta Petrologica Sinia, 33, 3422–3436 (in Chinese with English abstract).

Wang Q, Wyman DA, Xu JF, Zhao ZH, Jian P, Zi F. 2007a. Partial melting of thickened or delaminated lower crust in the middle of Eastern China: Implications for Cu-Au mineralization. The Journal of Geology, 115(2), 149–161. doi: 10.1086/510643.

Wang Q, Wyman DA, Xu JF, Jian P, Zhao ZH, Li CF, Xu W, Ma JL, He B. 2007b. Early Cretaceous adakitic granites in the Northern Dabie Complex, Central China: Implications for partial melting and delamination of thickened lower crust. Geochimica et Cosmochimica Acta, 71(10), 2609–2636. doi: 10.1016/j.gca.2007.03.008.

Wang Q, Xu JF, Zhao ZH, Bao ZW, Xu W, Xiong XL. 2004. Cretaceous high-potassium intrusive rocks in the Yueshan-Hongzhen area of East China: Adakites in an extensional tectonic regime within a continent. Geochemical Journal, 38(5), 417–434. doi: 10.2343/geochemj.38.417.

Wang Q, Xu JF, Zhao ZH, Xiong XL, Bao ZW. 2003. Petrogenesis of the Mesozoic intrusive rocks in the Tongling area, Anhui Province, China and their constraint on geodynamic process. Science in China Series D: Earth Sciences, 46(8), 801–815. doi: 10.1007/BF02879524.

Wang Q, Xu JF, Jian P, Bao ZW, Zhao ZH, Li CF, Xiong XL, Ma JL. 2006. Petrogenesis of adakitic porphyries in an extensional tectonic setting, Dexing, South China: Implications for the genesis of porphyry copper mineralization. Journal of Petrology, 47(1), 119–144. doi: 10.1093/petrology/egi070.

Wang SW, Zhou TF, Yuan F, Fan Y, White NC, Lin FJ. 2015. Geological and geochemical studies of the Shujiadian porphyry Cu deposit, Anhui Province, Eastern China: Implications for ore genesis. Journal of Asian Earth Sciences, 103, 252–275. doi: 10.1016/j.jseaes.2014.08.004.

Wang XL, Zhou JC, Wan YS, Kitajima K, Wang D, Bonamici C, Qiu JS, Sun T. 2013. Magmatic evolution and crustal recycling for Neoproterozoic strongly peraluminous granitoids from Southern China: Hf and O isotopes in zircon. Earth and Planetary Science Letters, 366, 71–82. doi: 10.1016/j.epsl.2013.02.011.

Wang Y, Tang DW, Xie JC. 2019. Geochemistry of apatite from Late Mesozioc intrusive rocks in Tongling area, Anhui Province: Constraints on rock-forming and ore-forming processes. Acta Petrologica et Mineralogica, 38, 63–76 (in Chinese with English abstract).

Wang Y, Yang XY, Deng JH. 2022a. Sr-Nd-Pb and zircon Hf isotopic constraints on the petrogenesis of two types of Early Cretaceous intrusive rocks in the Tongling ore-cluster region: Implications for Cu-Au polymetallic mineralization. Ore Geology Reviews, 150, 105122. doi: 10.1016/j.oregeorev.2022.105122.

Wang Y, Yang XY, Deng JH, Liu SS, Sun C, Hou Q, Wang LJ. 2022b. A comprehensive overview on the origin of intrusive rocks and polymetallic mineralization in the Tongling ore-cluster region, Lower Yangtze River Metallogenic Belt: Geological and geochemical constraints. Ore Geology Reviews, 141, 104625. doi: 10.1016/j.oregeorev.2021.104625.

Xie FW, Tang JX, Chen YC, Lang XH. 2018. Apatite and zircon geochemistry of Jurassic porphyries in the Xiongcun district, southern Gangdese porphyry copper belt: Implications for petrogenesis and mineralization. Ore Geology Reviews, 96, 98–114. doi: 10.1016/j.oregeorev.2018.04.013.

Xie JC, Wang Y, Li QZ, Liu JM, Yan J, Sun WD. 2018a. Early Cretaceous adakitic rocks in the Anqing region, southeastern China: Constraints on petrogenesis and metallogenic significance. International Geology Review, 60(11–14), 1435–1452. doi: 10.1080/00206814.2017.1362672.

Xie JC, Wang Y, Li QZ, Yan J, Sun WD. 2018b. Petrogenesis and metallogenic implications of Late Mesozoic intrusive rocks in the Tongling region, Eastern China: A case study and perspective review. International Geology Review, 60(11–14), 1361–1380. doi: 10.1080/00206814.2017.1386130.

Xie JC, Yang XY, Sun WD, Du JG. 2012a. Early Cretaceous dioritic rocks in the Tongling region, Eastern China: Implications for the tectonic settings. Lithos, 150, 49–61. doi: 10.1016/j.lithos.2012.05.008.

Xie JC, Chen S, Sun WD, Yang XY. 2012b. Geochemistry of Early Cretaceous adakitic rocks in Tongling region of Anhui Province: Constraints for rock-and ore-forming. Acta Petrologica Sinica, 28(10), 3181–3196 (in Chinese with English abstract).

Xie JC, Yang XY, Du JG, Sun WD. 2008. Zircon U-Pb geochronology of the Mesozoic intrusive rocks in the Tongling region: Implications for copper-gold mineralization. Acta Petrologica Sinica, 24, 1782–1800 (in Chinese with English abstract).

Xing K, Shu Q, Lentz DR, Wang F. 2020. Zircon and apatite geochemical constraints on the formation of the Huojihe porphyry Mo deposit in the Lesser Xing'an Range, NE China. American Mineralogist, 105, 382–396. doi: 10.2138/am-2020-7395.

Xu JF, Chen SS. 2023. Petrogenesis of adakitic rocks unrelated to slab melting and adakitic porphyries associated with Cu mineralization. Lithos, 458–459, 107351. doi: 10.1016/j.lithos.2023.107351.

Xu JF, Shinjo R, Defant MJ, Wang Q, Rapp RP. 2002. Origin of Mesozoic adakitic intrusive rocks in the Ningzhen area of East China: Partial melting of delaminated lower continental crust? Geology, 30(12), 1111. doi: 10.1130/0091-7613(2002)030<1111:oomair>2.0.co;2.

Xu XS. 2004. U-Pb dating of zircons from quartz diorite and its enclaves at Tongguanshan in Anhui and its petrogenetic implication. Chinese Science Bulletin, 49(19), 2073. doi: 10.1360/04wd0137.

Xu YM, Jiang SY, Zhu ZY, Yang SY, Zhou W. 2014. Petrogenesis of Late Mesozoic granitoids and coeval mafic rocks from the Jiurui district in the Middle–Lower Yangtze metallogenic belt of Eastern China: Geochemical and Sr–Nd–Pb–Hf isotopic evidence. Lithos, 190–191, 467–484. doi: 10.1016/j.lithos.2013.12.022.

Yan J, Liu J, Li Q, Xing G, Liu X, Xie J, Chu X, Chen Z. 2015. In situ zircon Hf–O isotopic analyses of late Mesozoic magmatic rocks in the Lower Yangtze River Belt, central eastern China: Implications for petrogenesis and geodynamic evolution. Lithos, 227, 57–76. doi: 10.1016/j.lithos.2015.06.010.

Yan J, Liu X, Wang S, Xie J, Liu J. 2021. Metallogenic type controlled by magma source and tectonic regime: Geochemical comparisons of Mesozoic magmatism between the Middle–Lower Yangtze River Belt and the Dabie Orogen, eastern China. Ore Geology Reviews, 133, 104095. doi: 10.1016/j.oregeorev.2020.104095.

Yang W, Zhang HF. 2012. Zircon geochronology and Hf isotopic composition of Mesozoic magmatic rocks from Chizhou, the Lower Yangtze Region: Constraints on their relationship with Cu–Au mineralization. Lithos, 150, 37–48. doi: 10.1016/j.lithos.2012.03.021.

Yang XY, Yang XM, Zhang ZW, Chi YY, Yu LF, Zhang QM. 2011. A porphyritic copper (gold) ore-forming model for the Shaxi-Changpushan district, Lower Yangtze metallogenic belt, China: geological and geochemical constraints. International Geology Review, 53, 580–611. doi: 10.1080/00206814.2011.562338.

Yang YZ, Chen FK, Siebel W, Zhang H, Long Q, He JF, Hou ZH, Zhu XY. 2014. Age and composition of Cu–Au related rocks from the lower Yangtze River belt: Constraints on paleo-Pacific slab roll-back beneath eastern China. Lithos, 202–203, 331–346. doi: 10.1016/j.lithos.2014.06.017.

Zhang CC, Sun WD, Wang JT, Zhang LP, Sun SJ, Wu K. 2017. Oxygen fugacity and porphyry mineralization: A zircon perspective of Dexing porphyry Cu deposit, China. Geochimica Et Cosmochimica Acta, 206, 343–363. doi: 10.1016/j.gca.2017.01.037.

Zhang H, Ling MX, Liu YL, Tu XL, Wang FY, Li CY, Liang HY, Yang XY, Arndt NT, Sun WD. 2013. High Oxygen Fugacity and Slab Melting Linked to Cu Mineralization: Evidence from Dexing Porphyry Copper Deposits, Southeastern China. Journal of Geology, 121, 289–305. doi: 10.1086/669045.

Zhang Q, Wang Y, Qian Q. 2001. The characteristics and tectonic-metallogenic significances of the adakites in Mesozoic period from eastern China. Acta Petrologica Sinica, 17, 236–244 (in Chinese with English abstract).

Zhang SY, Yang LQ, He WY, Gao X, Liu XD. 2021. Melt volatile budgets and magma evolution revealed by diverse apatite halogen and trace elements compositions: A case study at Pulang porphyry Cu-Au deposit, China. Ore Geology Reviews, 139, 104509. doi: 10.1016/j.oregeorev.2021.104509.

Zhang SB, Zheng YF. 2013. Formation and evolution of Precambrian continental lithosphere in South China. Gondwana Research, 23, 1241–1260. doi: 10.1016/j.gr.2012.09.011.

Zhang SB, Zheng YF, Wu YB, Zhao ZF, Gao S, Wu FY. 2006. Zircon isotope evidence for ⩾3. 5 Ga continental crust in the Yangtze craton of China. Precambrian Research, 146, 16–34. doi: 10.1016/j.precamres.2006.03.001.